Future Derecho Potential in the United States

KRISTIE KAMINSKI,[a] WALKER S. ASHLEY,[a] ALEX M. HABERLIE,[a] AND VITTORIO A. GENSINI[a]

[a] *Department of Earth, Atmosphere, and Environment, Northern Illinois University, DeKalb, Illinois*

(Manuscript received 17 October 2023, in final form 26 August 2024, accepted 9 October 2024)

ABSTRACT: This study uses high-resolution, convection-permitting, dynamically downscaled regional climate simulation output to assess how long-lived, convectively induced, extratropical windstorms known as derechos may change across the CONUS during the twenty-first century. Three 15-yr epochs including a historical period (1990–2005) and two separate late-twenty-first-century periods (2085–2100) employing intermediate (RCP4.5) and pessimistic (RCP8.5) greenhouse gas concentration scenarios are evaluated. A mesoscale convective system (MCS) identification and tracking tool catalogs derecho candidates across epochs using simulated radar reflectivity and maximum 10-m wind speed as a proxy for near-surface severe wind gusts. Results indicate that MCS-based windstorms, including derechos, are more frequent, widespread, and intense in both future climate scenarios examined for most regions of the central and eastern CONUS. Increases are suggested across all parts of the year, with significant changes in populations concentrated during the early spring and summer months, suggesting the potential for a longer, more extreme MCS windstorm season. This research provides insights for forecasters, emergency managers, and wind-vulnerable stakeholders on how these events may change across the twenty-first century so that they may mitigate, adapt to, and become resilient against severe convective storm perils.

SIGNIFICANCE STATEMENT: Long-lived, thunderstorm-induced, damaging wind events known as derechos may increase across most portions of the central and eastern United States in the future, with projections indicating a near doubling or tripling of annual cases in the Midwest, eastern Great Plains, and Mississippi and Ohio Valley regions by the end of the twenty-first century. Modeling projections suggest that future derechos could generally be longer-lived, more expansive, and capable of producing more severe wind gusts and damage, which will ultimately increase risk to life, infrastructure, and wind-sensitive industries affected by these extreme thunderstorm events.

KEYWORDS: Derecho; Severe storms; Squall lines; Climate change; Mesoscale systems

1. Introduction

A derecho is a long-lived, convectively induced windstorm associated with an extratropical mesoscale convective system (MCS) that produces severe wind gusts and an affiliated damage swath across an extensive area (Hinrichs 1888; Johns and Hirt 1987; Corfidi et al. 2016; Squitieri et al. 2023a). Due to their large size, speed, rapid onset, ferocity, and forecast difficulty, these events pose significant risk to life, infrastructure, and wind-sensitive industries (Ashley and Mote 2005; Squitieri et al. 2023a,b). Derechos can generate societal impacts equivalent to some landfalling hurricanes and large tornado outbreaks (Ashley and Mote 2005). For instance, the 2020 Corn Belt Derecho produced an estimated $13 billion (inflation adjusted to 2023 dollars) in damages making it the second costliest thunderstorm event on record behind the 25–28 April 2011 tornado outbreak sequence ($13.9 bn) and on par with many notable landfalling hurricanes (Smith and Katz 2013; Lasher-Trapp et al. 2023; NOAA NCEI 2023).

Increases in human and built-environment exposure in hazard-prone regions—known as the "expanding bullseye effect" (Ashley et al. 2014; Ashley and Strader 2016)—may explain some of the escalating frequency and magnitude of disasters such as the 2020 Corn Belt Derecho (Bundy et al. 2022). However, climate change may be an additional contributor to the evolving risk landscape of severe convective storm (SCS) events (Kunkel et al. 2013) and may play a role in the formation and maintenance of derechos by modifying the ingredients supportive of such events. The Intergovernmental Panel on Climate Change's Sixth Assessment Report (IPCC 2021) and others that have examined the relationship between anthropogenic climate change and SCSs conclude that environments favorable for SCSs—such as those that produce derechos—are likely to increase during the twenty-first century (Trapp et al. 2007; Brooks 2013; Diffenbaugh et al. 2013; Gensini et al. 2014; Gensini and Mote 2015; Tippett et al. 2015; Rasmussen et al. 2020; Lepore et al. 2021; Haberlie et al. 2022; Ashley et al. 2023). Derechos are produced by extratropical MCSs, which have been extensively researched (Houze 2004, 2018). However, this research has generally been motivated by improving understandings of changes in precipitation characteristics (Prein et al. 2017; Haberlie and Ashley 2019b; Schumacher and Rasmussen 2020), not convective wind. To date, there is little research assessing derecho climatology in the context of a changing climate.

The purpose of this study is to address the following research questions: 1) Can convection-permitting RCM (CP-RCM) output adequately replicate the climatology of CONUS derechos? 2) Using CP-RCM output, how is the derecho climatology

Supplemental information related to this paper is available at the Journals Online website: https://doi.org/10.1175/JCLI-D-23-0633.s1.

Corresponding author: Walker S. Ashley, washley@niu.edu

DOI: 10.1175/JCLI-D-23-0633.1

projected to change across the twenty-first century for various greenhouse gas emission trajectories? To answer these questions, convection-permitting dynamically downscaled output is employed for three 15-yr epochs including a historical period from 1990 to 2005 (HIST) and two late-twenty-first-century periods for 2085–2100 (FUTR) that were generated using RCP4.5 (FUTR 4.5) and RCP8.5 (FUTR 8.5). Simulation output variables, such as hourly maximum 10-m wind speed and composite radar reflectivity factor, are used in an updated version of an MCS identification and tracking tool (Haberlie and Ashley 2018a,b) to catalog derecho candidates that meet low-, medium-, and high-intensity thresholds (Coniglio and Stensrud 2004) across the simulation epochs. Event climatologies across the epochs are assessed for spatiotemporal changes, providing an initial set of perspectives on how these extreme wind events may change in the twenty-first century.

2. Background

a. *Derecho definition evolution*

Broadly, a derecho is a large, long-lived windstorm generated by a distinct form of the extratropical MCS—the quasi-linear convective system (QLCS). Hinrichs (1888) coined the term derecho in the late nineteenth century, but the modern definition evolved from Johns and Hirt (1987); they used Fujita and Wakimoto's (1981) downburst scale delineation of "family of downburst clusters" and certain length, longevity, and wind speed/damage report requirements as a basis to define the storms recognized by Hinrichs. Subsequent investigations of derecho climatology modified some of these criteria due to the quality, availability, and constraints of observational and severe report data required to define an event (Table 1; Bentley and Mote 1998; Bentley and Sparks 2003; Coniglio and Stensrud 2004; Ashley and Mote 2005; Guastini and Bosart 2016; Squitieri et al. 2023a). For example, concerns about nonmeteorological factors affecting wind report data—such as the extensive increase in reports following the implementation of the WSR-88D network and NWS warning verification program, potential sensitivity to population density, and known issues with estimated and measured wind gusts (Johns and Evans 2000; Doswell et al. 2005; Trapp et al. 2006; Edwards et al. 2018)—prompted investigations as to how altering the Johns and Hirt (1987) criteria may influence the resulting climatology of CONUS derechos (Bentley and Mote 2000; Johns and Evans 2000; Bentley and Sparks 2003; Coniglio and Stensrud 2004). While there are some differences depending on the criteria employed, current research agrees that derechos frequent two regions in the eastern CONUS: the upper Midwest through the Ohio Valley during the warm season and the southern Great Plains near Kansas and Oklahoma year-round, extending into the lower Mississippi Valley during the cool season (Johns and Hirt 1987; Bentley and Mote 1998; Bentley and Sparks 2003; Coniglio and Stensrud 2004; Coniglio et al. 2004; Ashley and Mote 2005; Corfidi et al. 2016; Guastini and Bosart 2016). More recently, a focus on the underlying and varying physical processes that generate these windstorms has led to a proposed revision to the derecho definition. Corfidi et al. (2016) argue for a more restrictive, dynamically reformed definition related to warm-season, progressive events; their definition requires events to illustrate on radar evidence of sustained bow echoes and/or rear-inflow jets. Thus, given the still-present debate in the literature (compare Squitieri et al. 2023a), research classifying derechos should be explicit about the definitional criteria employed, the constraints of the data used in that definition, and how changes to any of the criteria may have implications for the resulting climatology.

Derechos are generally classified into two categories based on large-scale environments and spatiotemporal damage patterns—serial or progressive (Johns and Hirt 1987). Serial derechos are associated with strong, synoptic-scale, surface low pressure systems, occur year-round, and produce wind damage primarily through the transfer of midtropospheric winds to the surface via convective downdrafts (Johns and Hirt 1987; Bentley and Mote 1998; Evans and Doswell 2001; Bentley and Sparks 2003; Corfidi et al. 2016). Progressive derechos—such as the 2020 Corn Belt Derecho—often have weaker dynamic forcing and, therefore, rely on subtle low-level thermodynamic instability for initiation, occur predominantly in the warm season, and produce swaths of significant wind damage through the formation of a rear-inflow jet, a strong cold pool, and convective downdrafts (Johns and Hirt 1987; Bentley and Mote 1998; Evans and Doswell 2001; Bentley and Sparks 2003; Corfidi et al. 2016; Guastini and Bosart 2016). A third "hybrid" classification has emerged to represent events that combine favorable environments and initiation mechanisms of serial and progressive events (Evans and Doswell 2001; Coniglio et al. 2004; Ashley et al. 2007; Squitieri et al. 2023b).

b. *Severe convective storms and anthropogenic climate change*

There is a growing body of literature linking potential changes in SCSs to anthropogenic climate change (Brooks 2013; Tippett et al. 2015; Allen 2018; Raupach et al. 2021; Gensini 2021), with international reports like the IPCC AR6 (IPCC 2021) and the 5th National Climate Assessment (USGCRP 2023) indicating that environments favorable for extreme weather, like SCSs, are likely to increase with warming. This finding is echoed in other works examining the relationship between anthropogenic climate change and SCSs, either, implicitly, through the use of GCMs to assess favorable environments or, explicitly, by using CP-RCMs that resolve convection at regional to local scales (Brooks 2013; Tippett et al. 2015; Allen 2018; Raupach et al. 2021; Gensini 2021). The implicit approach uses coarse GCM output to assess environmental ingredients supportive of convection, including moisture, instability, and wind shear (Marsh et al. 2007; Trapp et al. 2007, 2009; Diffenbaugh et al. 2013; Robinson et al. 2013; Gensini et al. 2014; Seeley and Romps 2015; Lepore et al. 2021). Results from this approach consistently suggest that environments supportive of SCSs are likely to increase during the twenty-first century (Brooks 2013; Tippett et al. 2015; Allen 2018; Raupach et al. 2021; Gensini 2021). However,

a corresponding increase in storm activity is not guaranteed due to other factors that influence SCS formation. An explicit approach uses high-resolution, but computationally expensive, CP-RCM output (Prein et al. 2015; Kendon et al. 2021; Lucas-Picher et al. 2021; Gensini et al. 2023) often generated by dynamical downscaling to explicitly simulate convection. When combined with storm-tracking techniques and other assessment tools, this approach can be used to draw conclusions about spatiotemporal distributions of various SCSs, with results, at least to date, suggesting that increases in frequency and seasonality are likely by the end of the twenty-first century (Trapp et al. 2011; Robinson et al. 2013; Gensini and Mote 2014, 2015; Trapp and Hoogewind 2016; Hoogewind et al. 2017; Rasmussen et al. 2020; Trapp et al. 2019; Gensini 2021; Haberlie et al. 2022; Ashley et al. 2023).

Although derechos can occur in a wide range of shear and instability environments (Evans and Doswell 2001; Squitieri et al. 2023b), future changes in tropospheric kinematics and thermodynamics due to anthropogenic climate change are likely to affect fundamental ingredients supportive (e.g., ample low-level moisture, unidirectional shear, and dry air aloft) of their formation and sustenance, which are expected to result in change in the overall climatology of these events. A recent study suggests that anthropogenic climate change may have contributed to the development and intensity of the southern European derecho of 18 August 2022 (González-Alemán et al. 2023). Another pseudo–global warming modeling approach investigating the 2020 Corn Belt Derecho suggests that an analogous event would likely affect a larger geographical area in the future due to changes in near-surface moisture and instability in a warming climate (Lasher-Trapp et al. 2023), consistent with findings that thunderstorm straight-line winds have intensified and affected a broader region in the central CONUS under climate change (Prein 2023). Conversely, a similar modeling approach found that future higher background values of instability and moisture may lead to weakening and/or premature decay of a mid-Atlantic derecho case since isolated deep convection ahead of the windstorm may affect sustenance under future warming (Li et al. 2023). While these recent case study approaches suggest climate change may modify—perhaps, in complex ways—future derechos and their environments, little research has systematically assessed potential climatological changes in a wind peril that has serious implications for life, industry, and infrastructure. We use this void in the literature as a catalyst to examine the relationship between anthropogenic climate change and CONUS derecho climatology.

3. Data and methods

a. *Regional climate model output*

Data for this study are derived from CP-RCM simulations generated by Gensini et al. (2023). They used the WRF-ARW v4.1.2 in a convection-permitting configuration over the CONUS, with horizontal grid spacing of 3.75 km, 51 vertical levels, and a data output interval of 15 min. Initial and lateral boundary conditions are forced by GCM data, specifically NCAR's CESM that participated in phase 5 of the Coupled Model Intercomparison Project (CMIP5), which were regridded and bias corrected (Bruyère et al. 2014, 2015) using 1981–2005 ERA-Interim reanalysis (Dee et al. 2011). Bias correction improves overall simulation performance by reducing errors that could be passed from GCMs into a CP-RCM simulation during dynamical downscaling (Christensen et al. 2008). Simulations also utilized spectral nudging (Miguez-Macho et al. 2004) at 6-hourly intervals for synoptic-scale features above the planetary boundary layer.

Gensini et al. (2023) simulation output verified well against assimilated observations (Daly et al. 1994) of temperature and precipitation with only slight seasonal and regional biases and has been used in other studies examining intersections of anthropogenic climate change with thunderstorm (Haberlie et al. 2022), MCS (Haberlie et al. 2023), and supercell activity (Ashley et al. 2023). The reduction in warm and dry biases in the Great Plains in the Gensini et al. (2023) dataset in contrast to other dynamically downscaled simulations used to investigate QLCS projections (Liu et al. 2016; Haberlie and Ashley 2019b) may permit more accurate representations of MCS/QLCS climatologies. For further model configuration and verification information, please see Gensini et al. (2023).

b. *10-m wind speed (over the previous hour)*

The Air Force Weather Agency (AFWA) maximum 10-m wind speed (m s^{-1}) over the previous hour (WSPD10MAX; Creighton et al. 2014) is used as a proxy for near-surface severe wind gusts when identifying derecho candidates. In convective instances (when precipitation rates are greater than 50 mm h^{-1}), WSPD10MAX is calculated by blending upper-level winds (1 km AGL) with surface-level winds to account for increased gust potential when precipitation is heavy and when winds are strong aloft. Calculated WSPD10MAX values are then used to parameterize surface wind gusts following a Weibull distribution algorithm that accounts for differences in gust potential over land and water (compare Creighton et al. 2014). For a complete derivation of 10-m wind in WRF-ARW with selected microphysics and parameterization schemes as described in Gensini et al. (2023), please see Skamarock et al. (2019).

Research verifying the accuracy of modeled wind gusts against observations has displayed mixed results due to differences in model parameterization, microphysics, and initial and lateral boundary conditions (Adams-Selin et al. 2013; Zhang et al. 2013; Figurski et al. 2022; Shepherd et al. 2021; Liu et al. 2023), the model's ability to accurately resolve localized mesoscale features (Zhang et al. 2013; Sheridan 2018; Jung et al. 2022), or differences between diurnal or synoptic weather conditions (Sheridan 2018; Lang et al. 2022). While verification of AFWA 10-m wind gusts is not the intention of this study, the distribution of WSPD10MAX gusts meeting, or exceeding, the minimum severe threshold of 25.7 m s^{-1} is assessed to identify regions where using this variable as a proxy for potentially damaging wind swaths may overestimate or underestimate severe wind-producing MCS frequency. The

TABLE 1. A summary of previous derecho climatologies for the CONUS including years examined (*warm season only), number of events (**progressive only), criteria used to identify derechos, and spatial findings. Adapted from Coniglio and Stensrud (2004; their Table 1) and Guastini and Bosart (2016; their Table 1).

	Johns and Hirt (1987) (JH87)	Bentley and Mote (1998) (BM98)	Bentley and Sparks (2003) (BS03)	Coniglio and Stensrud (2004) (CS04)	Ashley and Mote (2005)	Guastini and Bosart (2016) (GB16)
Years	1980–83*	1986–95	1986–2000	1986–2001	1986–2003	1996–2013*
Events	70	112	230	244	377	256**
1	There must be a concentrated area of convectively induced wind gusts greater than 26 m s^{-1} that has a major axis length of 400 km or more	As in JH87	As in JH87	As in JH87	As in JH87	As in JH87
2	The wind reports must have chronological progression	As in JH87	As in JH87	As in JH87	As in JH87	As in JH87
3	No more than 3 h can elapse between successive wind reports	No more than 2 h can elapse between successive wind reports	As in BM98	No more than 2.5 h can elapse between successive wind reports	As in CS04	As in CS04
4	There must be at least three reports of either F1 damage or wind gusts greater than 33 m s^{-1} separated by at least 64 km during the MCS stage of the event	Not used	As in BM98	Low end, not used; moderate, same as in JH87; high end, there must be at least three reports of either wind gusts greater than 38 m s^{-1} or comparable damage, at least two of which must occur during the MCS stage of the event	As in BM98	As in BM98
5	The associated MCS must have spatial and temporal continuity	The associated MCS must have spatial and temporal continuity with no more than 2° of latitude and longitude separating successive wind reports	As in BM98	The associated MCS must have spatial and temporal continuity, and each report must be within 200 km of the other reports within a wind gust swath	As in BM98	As in CS04
6	Multiple swaths of damage must be part of the same MCS as indicated by the available radar data	Multiple swaths of damage must be part of the same MCS as seen by temporally mapping the wind reports of each event	As in BM98	As in JH87	As in JH87	As in JH87
Spatial maximum	Upper Midwest through the Ohio Valley	Southern Great Plains eastward through Missouri and southeastward through Louisiana; secondary maximum in the Ohio Valley	Northern Great Plains through the Ohio Valley; secondary maximum in the southern Great Plains	Southern Great Plains; upper Mississippi River valley into Ohio	Southern Great Plains southeastward through the Mississippi River valley; upper Midwest through the Ohio Valley	Southern Minnesota to Ohio/West Virginia border; secondary maximum in Kansas and Oklahoma

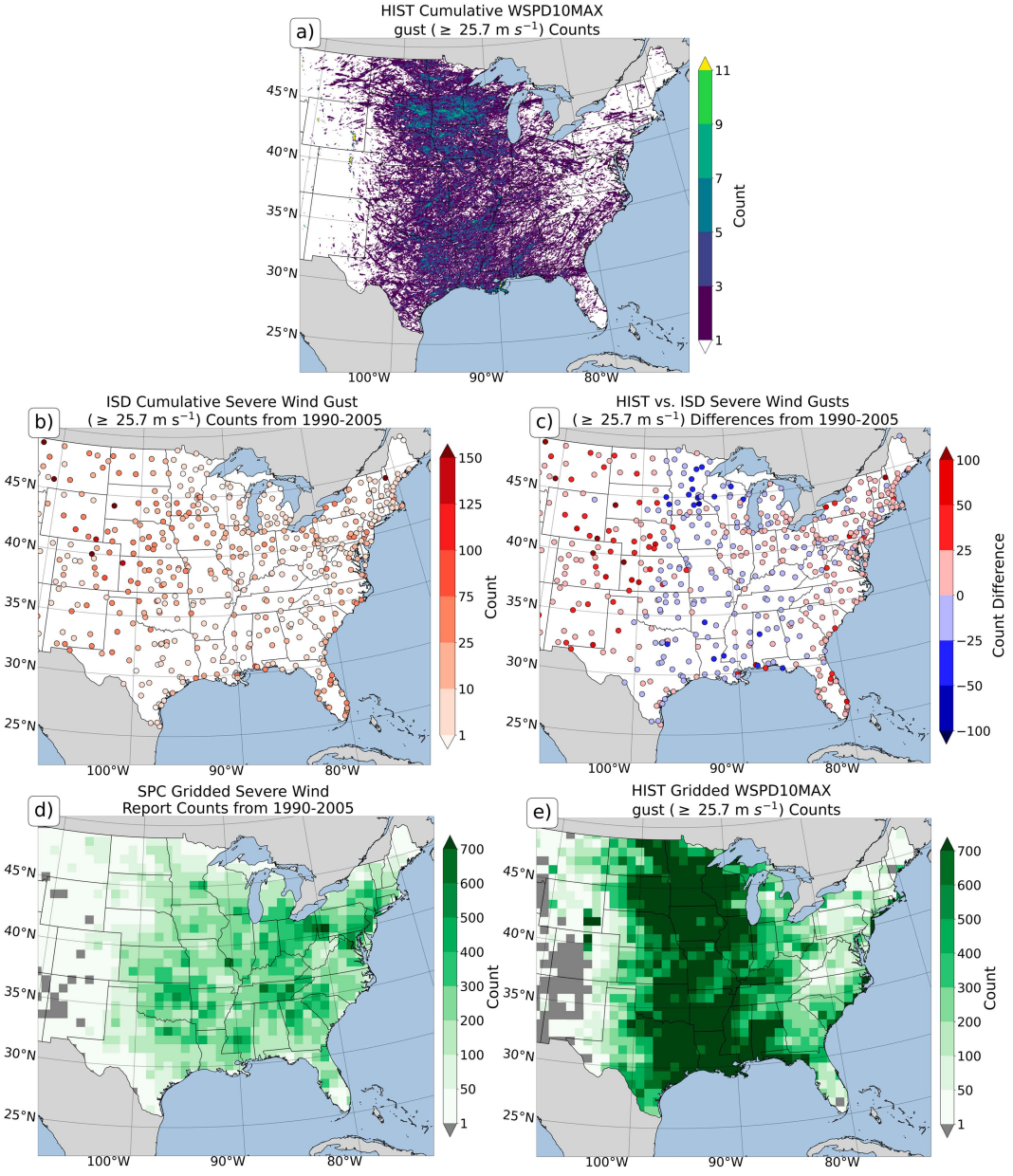

FIG. 1. Spatial evaluation of (a) HIST WSPD10MAX severe gust data against observed severe gusts from (b) NCEI's global hourly ISD and (d) the SPC's estimated and observed severe wind gusts, as well as damage reports, for 1990–2005. (c) Differences in observed and modeled severe gust counts using a summed nearest neighbor approach. Red shades indicate stations with higher observed severe wind gusts, while blue shades indicate stations with lower observed severe wind gusts when compared to HIST WSPD10MAX severe gusts. (e) The counts shown in (a), but on an 80-km grid.

only study to use WRF 10-m wind gusts as a proxy for forecasting severe wind-producing MCSs concluded that the model tended to overestimate low wind speeds and underestimate high wind speeds when compared to observations (Milne 2016).

c. *10-m severe wind comparison*

Only 0.0009% (1 515 993) of all HIST WSPD10MAX values (1.65×10^{11} values total) are ≥25.7 m s^{-1}, ranging from 0.0003% to 0.002% annually, with a mean of 0.0009%. Approximately 34.2% of grid cells in the simulation domain experience at least one severe HIST WSPD10MAX gust, annually ranging from 1.8% to 8.4% with a mean of 4.5%. Regions of counts exceeding one severe gust per grid cell are unsurprisingly concentrated over bodies of water and mountainous regions (not shown), but other small-scale, localized regions exist throughout the upper Midwest and the southern Great Plains (Fig. 1a). HIST WSPD10MAX gusts that meet, or exceed, the minimum severe wind gust threshold of

TABLE 2. Criteria used to identify low, moderate, high-end wind, and derecho (i.e., moderate and high-end) events from MCS slices and swaths generated using dynamically downscaled RCM output. Derived from criteria presented in Table 1. Adapted from Ashley et al. (2005, their Table 2) and Ashley and Mote (2005, their Table 1).

Minimum length	There must be a concentrated area of wind gusts greater than 26 m s^{-1} that has a major axis length of 400 km or more
Chronological progression	Wind gusts must have chronological progression, either as a singular swath (progressive) or as series of swaths (serial)
Temporal and spatial restrictions	No more than 3 h can elapse between successive wind gusts, with no more than 2 degrees of latitude and longitude separating successive wind gusts
Origin of wind swath	Multiple swaths of gusts must be part of the same MCS swath as indicated by examining simulated radar reflectivity
MCS swath continuity	The associated MCS swath must have temporal and spatial continuity (as indicated by examining simulated radar reflectivity)
Land restriction	A wind swath attributed to an MCS swath must intersect the CONUS
Intensity thresholds	Low end: meets above
	Moderate: There must be at least three wind gusts greater than 33 m s^{-1} separated by 64 km or more that occur within the MCS swath
	High end: There must be at least three wind gusts greater than 38 m s^{-1}, at least two of which must occur within the MCS swath

25.7 m s^{-1} are compared against two sources (Figs. 1b–d): NCEI's Global Hourly Integrated Surface Database (ISD; Smith et al. 2011) and severe wind reports from the Storm Prediction Center's (SPC) Severe Weather Database (https://www.spc.noaa.gov/wcm/#data). Issues for both databases are well documented in the literature; surface observation wind gust data from ISD sites may be measured using inconsistent sampling periods or may not be reported due to varying regional requirements (Harper et al. 2010; Suomi et al. 2015; Harris and Kahl 2017; Lang et al. 2022), whereas wind reports are subject to bias and can be influenced by nonmeteorological factors (Johns and Evans 2000; Weiss et al. 2002; Doswell et al. 2005; Trapp et al. 2006; Smith et al. 2013; Edwards et al. 2018). Despite noted shortcomings, these datasets are some of the only verification options available for the period of record overlapping the HIST climate simulation. No adjustments are made to quality control the data or remove nonconvective wind gusts. Therefore, this study used 421 CONUS ISD sites with complete hourly wind gust data and 93 421 severe wind reports that occurred between 1 October 1990 and 30 September 2005. To combat resolution differences between the CP-RCM output and the ISD site data, the sum of HIST WSPD10MAX gusts in a 3 × 3 (11.25 km × 11.25 km) gridcell array approximately centered over each ISD site is calculated. Comparisons between SPC severe wind reports and HIST WSPD10MAX severe gusts are conducted on an 80 km × 80 km grid.

The historical simulation generates more severe wind gusts across the upper Midwest and portions of the Deep South, and fewer gusts throughout the northeast and most of the western Great Plains, especially near the Front Range, compared to the ISD site data (Figs. 1b,c). While gridded HIST WSPD10MAX severe counts and SPC wind reports share a spatial maximum over the Ark-La-Tex region (Figs. 1d,e), the simulation data do not reflect the two wind report maxima over eastern Tennessee and the Ohio Valley (Fig. 1d) and, instead, concentrate severe gusts over a broad region of the central United States, extending from Texas to Minnesota (Fig. 1e). With both datasets considered, higher counts across the Midwest and lower counts across the western Great Plains and northeast extending southward through the Appalachian region may help explain potential deviations of the historical simulation from observed climatologies, since severe wind gusts are the basis for extracting damaging wind swaths from MCS swaths (Table 2).

d. *Derecho identification and tracking*

MCSs and QLCSs have been manually or automatically identified, tracked, and cataloged by examining precipitation or cloud clusters that meet defined criteria thresholds (Parker and Johnson 2000; Houze 2004) using observed or simulated radar reflectivity (Haberlie and Ashley 2018a,b; Ashley et al. 2019; Haberlie and Ashley 2019a,b; Surowiecki and Taszarek 2020; Cui et al. 2021) or satellite imagery (Cheeks et al. 2020; Núñez Ocasio et al. 2020; Feng et al. 2021). Image segmentation and storm tracking (Lakshmanan and Smith 2010) have become a popular approach to MCS/QLCS identification especially when combined with supervised machine learning (Theodoridis and Koutroumbas 2003) as they permit efficient processing of a large volume of data in a short amount of time (Lakshmanan and Smith 2009). Here, MCSs are identified and tracked via the methods initially presented in Haberlie and Ashley (2018a,b) and applied to the Gensini et al. (2023) dataset in Haberlie et al. (2023). In this approach, the image segmentation process [following criteria presented by Parker and Johnson (2000)] uses composite radar reflectivity factor (column maximum radar reflectivity derived from the Thompson microphysics scheme; Thompson et al. 2008) to aggregate convective pixels (≥40 dBZ) within 24 km of each other into contiguous regions. Regions that have a major axis length of 100 km or greater are attached to surrounding stratiform precipitation (≥20 dBZ) within 96 km to form MCS slices (Haberlie and Ashley 2018a). Slices are then spatiotemporally merged, and the subset of swaths that last for at least 3 h are retained as MCS swaths (Haberlie and Ashley 2018b). For detailed

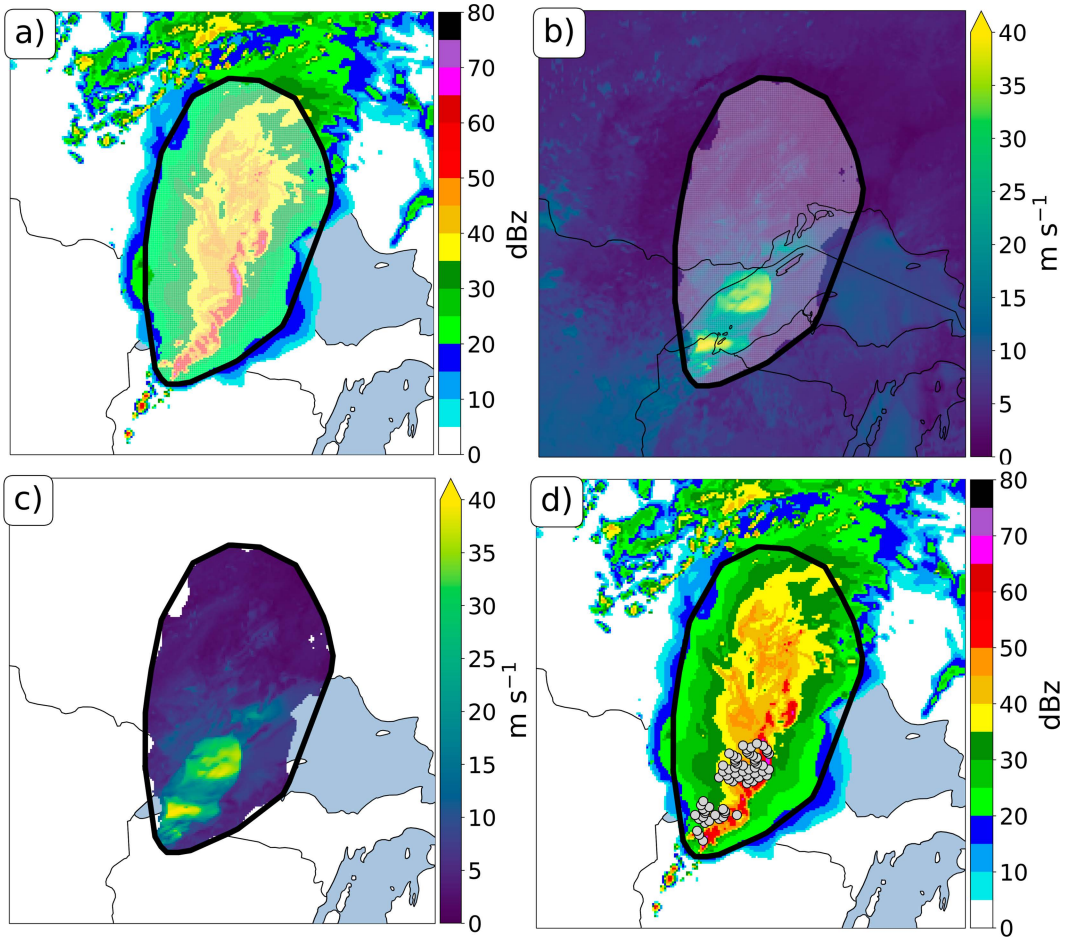

FIG. 2. A visual demonstration of the process used to attribute WSPD10MAX gusts to hourly MCS slices. (a) The convex hull (e.g., black polygon) is generated around a sample MCS slice from 0000:00 UTC 1 Sep 1991 and over (b) the corresponding WSPD10MAX field for this time step. (c) The WSPD10MAX values occurring within the convex hull are extracted, and (d) values greater than 25.7 m s^{-1} are annotated as gray points. Only 66 (10%) of the 660 severe wind gusts for this time step are annotated in (d) due to the high spatial resolution of the simulation output.

information related to the segmentation and tracking approach, and a discussion of known issues associated with storm tracking, please see Haberlie and Ashley (2018a,b) and Haberlie et al. (2023).

While studies using observed or simulated reflectivity data with a semi- or fully automated tracking approach are present in the literature (Haberlie and Ashley 2018a,b; Ashley et al. 2019; Haberlie and Ashley 2019a,b), no methods have used wind threshold criteria in conjunction with tracking. That said, Ashley et al. (2019) did use a buffering technique to attribute severe wind gust and/or damage reports from the SPC's GIS-ready severe report database (www.spc.noaa.gov/gis/svrgis) to investigate QLCS events. Here, the convex hull of each MCS slice (Fig. 2a) is large enough to sufficiently capture (Fig. 2b) and attribute grid cells experiencing severe WSPD10MAX gusts to their parent MCS slice (Fig. 2c). Buffering around the convex hull is not necessary since gusts are the maximum over the previous hour and therefore do not occur in front of ongoing convection. This process was repeated for each slice within a MCS swath, effectively generating an array of severe wind points (Fig. 2d), upon which spatiotemporal operations that assess metrics like major axis length, area, and continuity can be performed to generate and validate damaging wind swaths (Figs. ES1 and ES2 in the online supplemental material).

MCS swaths, and their respective wind swaths, that met modified derecho criteria as presented in Table 2 [based on criteria determined by Fujita and Wakimoto (1981), Johns and Hirt (1987), and Coniglio and Stensrud (2004)] are retained as potential derecho candidates. To avoid capturing only extreme derechos, and to communicate the spectrum of change possible for all MCS-based straight-line windstorms, the low-end, moderate, and high-end criteria presented by Coniglio and Stensrud (2004) are employed. These events are not a one-to-one recreation of observed CONUS derechos—a limitation of the dynamically downscaled approach—and, accordingly, are compared to observed spatiotemporal patterns during the period overlapping the historical epoch. We caution the reader that the simulated

low-end, moderate, high-end, and derecho MCS swaths analyzed should be treated as proxies for the "real-world" occurrence of these events. Although they satisfy the requirements outlined in Table 2, a one-to-one validation to observed events is not feasible due to methodological disparities (such as an objective tracking approach vs subjective interpretation of criteria for event footprint generation) and differences in the underlying wind data (e.g., gridded wind data vs reliance on a sparse wind observation network, including reports). That said, a comparison to previous work is still provided to assess the performance of the detection and tracking approach, but the differences in the data and techniques underpinning the event definition heavily influence this comparison, particularly regional frequency. The climatological changes presented in the later sections are not contingent on this comparison since the low-end, moderate, high-end, and derecho MCS swaths are treated as proxies for activity and should be interpreted as potential changes between a historical baseline and future climate scenarios.

4. Results and discussion

a. *Historical simulation and observed derecho comparison*

There are 13 224 detected MCS swaths whose spatial extent intersected the CONUS during the historical epoch, with a mean of 881 per hydrologic year, ranging from a minimum of 779 in 1990–91 and a maximum of 1004 in 1996–97 (Table 3). Annual, and cumulative, counts are likely higher than those observed in Haberlie and Ashley (2019a) since efforts to reduce the inclusion of non-MCS events not removed by image processing alone (such as hurricanes and unorganized clusters of convective cells) were not performed. However, these event types are generally removed when low-end, moderate, and high-end criteria are implemented, as unorganized convective clusters do not consistently produce severe wind gusts across the required spatial and temporal domains (Table 2), and severe wind swaths attributed to tropical cyclone activity are concentrated over ocean basins. Of the MCS swaths, approximately 28% (3710) produce at least one severe wind gust (Table 3). While not every simulated severe wind MCS swath meets the criteria classification of a QLCS, Ashley et al. (2019) suggested that approximately 27% of observed MCSs categorized as QLCSs can be linked to a severe wind report, broadly aligning with the proportion suggested here. Upon implementation of low-end criteria, the percentage drops to 6.6% (873), suggesting most simulated MCS swaths do not produce spatially concentrated or temporally continuous severe wind swaths. Only 2.4% (318) of MCS swaths went on to meet moderate criteria, and approximately 0.7% (89) satisfied high-end criteria. Of the 873 MCS swaths that meet at least low-end criteria, 63.5% (555) meet strictly low-end criteria, 25.2% (229) are classified as moderate, and 11.2% (89) meet high-end requirements resulting in a mean of 37, 15.3, and 5.9 events per simulation year, respectively (Table 4). Past derecho climatologies have employed the low-end (Bentley and Mote 1998; Bentley and Sparks 2003; Coniglio and Stensrud 2004; Ashley and Mote 2005) or moderate thresholds (Johns and Hirt 1987) as minimum derecho criteria; doing so here yields a mean count of 58.2 and 21.2 derechos per year. To be consistent with the annual means observed in previous studies (Table 4), and to restrict the sample to MCS swaths more likely to emanate progressive characteristics consistent with a newer, dynamically based definition (Corfidi et al. 2016), derecho events are defined as those that meet moderate or high-end wind swath criteria. Excluding low-end MCS swaths may yield lower derecho frequencies across the Southern Plains, Arkansas River region, and the Mississippi and Ohio River valleys (Coniglio and Stensrud 2004).

The spatiotemporal distributions of HIST low-end, moderate, and high-end MCS swaths compare reasonably well against observed climatologies considering the underlying differences in simulated and observed wind and the use of an automated, nonsubjective tracking approach. HIST low-end, moderate, and high-end MCS swaths occurred primarily during the warm season (May–August) with an absolute peak in June and July (Figs. 3a–i and 4a–f). On an annual basis, HIST MCS swaths meeting low-end criteria frequent the southern Great Plains, specifically Kansas and Oklahoma, with a secondary maximum along the Eastern Seaboard near the Carolinas (Fig. 5a). This secondary spatial maximum is likely due to the algorithm's ability to capture all severe wind MCS swaths that intersect the CONUS; convection that moves over the Atlantic and begins producing severe wind gusts along the coast is retained here but is likely not in a climatology based on observed severe wind reports. Spatial patterns in the warm and cool seasons (September–April) approximate those produced by Coniglio and Stensrud (2004; their Figs. 5a and 9a) with most warm-season events concentrated across the central and southern Great Plains (Fig. 6a) and cool-season events maximized over the Ark-La-Tex region, extending eastward into Mississippi (Fig. 7a). Similarly, two corridors of maximum frequency are observed for moderate and high-end MCS swaths: throughout the central Great Plains and upper Midwest extending eastward toward the Ohio Valley during the warm season (Figs. 6d,g) and across the Deep South during the cool season (Figs. 7d,g). This spatial pattern echoes that presented by Coniglio and Stensrud (2004; their Figs. 5b,c and 9b,c), with small differences in the northward extent of activity during the cool season.

The HIST derecho (i.e., moderate and high-end MCS swaths) climatology is representative of observed CONUS derechos (Coniglio et al. 2004; Ashley and Mote 2005). Both the northern and southern corridors of activity are captured: throughout the Midwest extending southeastward toward the Ohio Valley and in the Ark-La-Tex region extending eastward along the Gulf Coast States (Fig. 5j). The northern maximum does not extend as far east into the Appalachian region compared to Coniglio and Stensrud (2004) and Ashley and Mote (2005), and this is likely the result of excluding low-end MCS swaths or noted lower severe wind gust counts across the northeast CONUS (Figs. 1c,e). Additionally, the southern maximum is displaced from Kansas/Oklahoma southward, which, again, is likely a combination of excluding low-end MCS swaths and the algorithm's ability to track severe wind-producing MCS swaths over the Gulf of Mexico due to high-

TABLE 3. Annual count of MCS swaths as well as the count and proportion of annual MCS swaths that produced severe wind, or produced a severe wind swath meeting at least low-end, moderate, or high-end criteria for (top) HIST, (middle) FUTR 4.5, and (bottom) FUTR 8.5 for the CONUS. Boldface values indicate the maximum value for that column. An event that produces a wind swath meeting high-end criteria as outlined in Table 2 is counted in each preceding category (moderate, low end, and severe wind); categories are cumulative.

		Severe wind		Low end		Moderate		High end	
HIST	Total MCS	MCS count	MCS %	MCS count	MCS %	MCS count	MCS %	MCS count	MCS %
1990–91	779	222	28.50	42	5.39	14	1.80	4	0.51
1991–92	828	165	19.93	38	4.59	8	0.97	2	0.24
1992–93	913	240	26.29	42	4.60	12	1.31	5	0.55
1993–94	798	214	26.82	45	5.64	19	2.38	4	0.50
1994–95	796	262	**32.91**	57	7.16	26	3.27	8	1.01
1995–96	941	269	28.59	70	7.44	27	2.87	9	0.96
1996–97	**1004**	**322**	32.07	71	7.07	28	2.79	3	0.30
1997–98	934	258	27.62	**74**	7.92	**32**	**3.43**	**12**	**1.28**
1998–99	937	258	27.53	66	7.04	30	3.20	8	0.85
1999–2000	936	237	25.32	57	6.09	19	2.03	5	0.53
2000–01	880	259	29.43	64	7.27	24	2.73	7	0.80
2001–02	909	239	26.29	68	7.48	18	1.98	7	0.77
2002–03	805	251	31.18	62	7.70	21	2.61	5	0.62
2003–04	945	272	28.78	48	5.08	14	1.48	3	0.32
2004–05	819	242	29.55	69	**8.42**	26	3.17	7	0.85
Total	13 224	3710	28.06	873	6.60	318	2.40	89	0.67
FUTR 4.5	Total MCS	MCS count	MCS %	MCS count	MCS %	MCS count	MCS %	MCS count	MCS %
2085–86	870	334	38.39	74	8.51	31	3.56	11	1.26
2086–87	792	240	30.30	62	7.83	25	3.16	8	1.01
2087–88	996	347	34.84	77	7.73	31	3.11	19	1.91
2088–89	813	271	33.33	67	8.24	29	3.57	7	0.86
2089–90	939	361	38.45	104	11.08	43	4.58	16	1.70
2090–91	970	303	31.24	73	7.53	37	3.81	15	1.55
2091–92	**1030**	**399**	**38.74**	**135**	**13.11**	**70**	**6.80**	**26**	**2.52**
2092–93	904	327	36.17	99	10.95	55	6.08	13	1.44
2093–94	958	345	36.01	106	11.06	44	4.59	17	1.77
2094–95	1011	328	32.44	86	8.51	38	3.76	9	0.89
2095–96	1020	342	33.53	82	8.04	35	3.43	8	0.78
2096–97	889	317	35.66	101	11.36	45	5.06	17	1.91
2097–98	988	302	30.57	70	7.09	24	2.43	6	0.61
2098–99	1013	333	32.87	94	9.28	49	4.84	24	2.37
2099–2100	968	276	28.51	72	7.44	29	3.00	5	0.52
Total	14 161	4825	34.07	1292	9.12	575	4.06	201	1.42
FUTR 8.5	Total MCS	MCS count	MCS %	MCS count	MCS %	MCS count	MCS %	MCS count	MCS %
2085–86	908	371	40.86	110	12.11	57	6.28	23	2.53
2086–87	967	413	42.71	109	11.27	53	5.48	21	2.17
2087–88	**1178**	454	38.54	121	10.27	58	4.92	22	1.87
2088–89	944	384	40.68	97	10.28	45	4.77	21	2.22
2089–90	845	344	40.71	118	13.96	57	6.75	23	2.72
2090–91	1079	466	43.19	135	12.51	64	5.93	21	1.95
2091–92	1035	419	40.48	109	10.53	62	5.99	**32**	3.09
2092–93	1162	447	38.47	109	9.38	56	4.82	21	1.81
2093–94	1004	423	42.13	118	11.75	57	5.68	23	2.29
2094–95	972	407	41.87	116	11.93	62	6.38	24	2.47
2095–96	1048	435	41.51	107	10.21	52	4.96	24	2.29
2096–97	1084	**473**	43.63	**138**	12.73	65	6.00	30	2.77
2097–98	853	375	**43.96**	128	**15.01**	**69**	**8.09**	31	**3.63**
2098–99	847	320	37.78	89	10.51	44	5.19	19	2.24
2099–2100	923	365	39.54	105	11.38	53	5.74	23	2.49
Total	14 849	6096	41.05	1709	11.51	854	5.75	358	2.41

TABLE 4. Comparison of HIST low-end, moderate, and high-end MCS swath counts to previous CONUS derecho climatologies (* indicates a study conducted for the warm season only and ** indicates a study conducted for progressive derechos only). Article labeling as in Table 1.

	Number of events	Length of dataset (years)	Mean number of events per year
JH87*	70	4	17.5
BM98	112	10	11.2
BS03	230	15	15.3
CS04	244	16	15.3
AM05	377	18	20.9
GB16*,**	256	18	14.2
HIST low end	555	15	37.0
HIST moderate	229	15	15.3
HIST high end	89	15	5.9
Total	873	15	58.2
HIST moderate + high end	318	15	21.2

resolution wind gust coverage. Derechos predominantly occur during the warm season (Figs. 3k,l and 4g), with a peak of five mean events in both June and July, which aligns well with monthly counts found by Ashley and Mote (2005; their Fig. 3). Derecho activity is concentrated over the Midwest and central Great Plains during the warm season (Fig. 6j) and across the Deep South extending northward into the Midwest during the cool season (Fig. 7j).

b. *Spatial and temporal changes*

MCS swath activity increases across the CONUS in both the FUTR 4.5 and 8.5 epochs, with the largest increases noted for the pessimistic simulation. The FUTR 4.5 (FUTR 8.5; parenthetically referenced henceforth) scenario generates 14 161 (14 849) MCS swaths that intersect the CONUS, a 7% (12%) increase from HIST (Table 3). However, MCS swaths in each category (Table 2) do not increase following these proportions, suggesting severe straight-line wind may become a more prominent hazard in future climates. Approximately 34% (41%) of MCS swaths produce at least one severe wind gust, a 30.1% (64.3%) increase compared to HIST. Similarly, 9.1% (11.5%) of MCS swaths meet at least low-end criteria, a 47.9% (95.8%) increase, 4.1% (5.8%) meet at least moderate criteria, an 80.8% (168.6%) increase, and 1.4% (2.4%) meet high-end criteria, a 125.8% (302.2%) increase (Table 3). Increasing activity across the Ozark, mid-South, and Gulf Coast regions (Fig. 5), especially in the cool and transition seasons (Figs. 6 and 7), where climatological prevalence of low-CAPE, high-shear environments (Burke and Schultz 2004; Sherburn and Parker 2014; Sherburn et al. 2016), and/or frontal forcing associated with migrating extratropical systems (Whittaker and Horn 1984; Bengtsson et al. 2006; Fritzen et al. 2021) may support more frequent linear convection and, therefore, severe wind (Smith et al. 2012, 2013; Ashley et al. 2019).

Mean and median low-end, moderate, and high-end counts, including derechos, increase at annual, seasonal, and monthly scales (Figs. 3, 4, and 8, Table 5, Fig. ES3, Tables ES1–ES4) throughout the eastern CONUS between the HIST and FUTR epochs (Figs. 5–7), with the highest positive deltas observed for the FUTR 8.5 scenario. Diurnally, these events remain a late afternoon and evening threat regardless of simulation epoch (Fig. 9). Other characteristics such as duration, cumulative wind swath area, and the count of grid cells experiencing severe, significant severe, and extreme wind gusts (within a wind swath) were assessed as proxies for intensity (Table 5, Fig. 8, Tables ES1–ES4). Many changes are statistically significant via the Mann–Whitney U test ($p < 0.05$), which is often used to assess differences in population shape for small samples (here, $n = 15$). The reader should be mindful when interpreting significant changes, noting that 15 years is a relatively small sample size to capture shifts in activity with such low annual counts compared to other SCS types (Haberlie et al. 2022; Ashley et al. 2023).

1) LOW-END MCS SWATHS

Mean annual low-end MCS swath counts increase across the mid-South for future epochs, extending northeastward across the Appalachian region into New England (Figs. 5b,c). These changes are driven by decreasing warm-season events across the Great Plains and Midwest (Figs. 6b,c), more cool-season events across the Ozarks and the mid-South (Figs. 7b,c), and for FUTR 8.5, higher mean counts east of 90°W during the warm season. The largest positive mean deltas tend to overlap areas with significant ($p < 0.05$ via Mann–Whitney U test) population changes; low-end MCS swath population differences are significant across the mid-South and Ozark regions in the cool season and for FUTR 8.5 in the warm season (Figs. 5b,c, 6b,c, and 7b,c). Further, low-end MCS swaths occur more frequently in the future climate simulations, with mean (median) counts increasing from 37 (38) events in HIST to 47.8 (46) events in FUTR 4.5 and 57 (55) events in FUTR 8.5 (Figs. 3a and 8a, Table 5, Table ES1). Although they remain a warm-season phenomenon, peaking in June and July across HIST and both FUTR epochs, significant population differences are observed during the warm and transition seasons (Figs. 3b,c and 4a,b, Fig. ES3a, Table ES1), suggesting a longer and more active window for low-end MCS swaths. While changes for different characteristics are noted, no clear signals emerge from significance testing (Figs. 8b,c, Table 5, Table ES1).

2) MODERATE MCS SWATHS

MCSs that produce a severe wind swath meeting moderate criteria increase across a broad region encompassing the southern Great Plains through New England, with localized areas of decreasing mean annual counts across the Midwest (Figs. 5e,f). Unlike low-end MCS swaths, spatial changes for both scenarios are driven by increases across a northern corridor extending from the Midwest into the Ohio Valley during the warm season (Figs. 6e,f) and throughout a southern corridor concentrated in the Deep South for FUTR 4.5 (Fig. 7e) and the Ozark Plateau for FUTR 8.5 (Fig. 7f) during the cool season. Like low-end events, significant changes in moderate

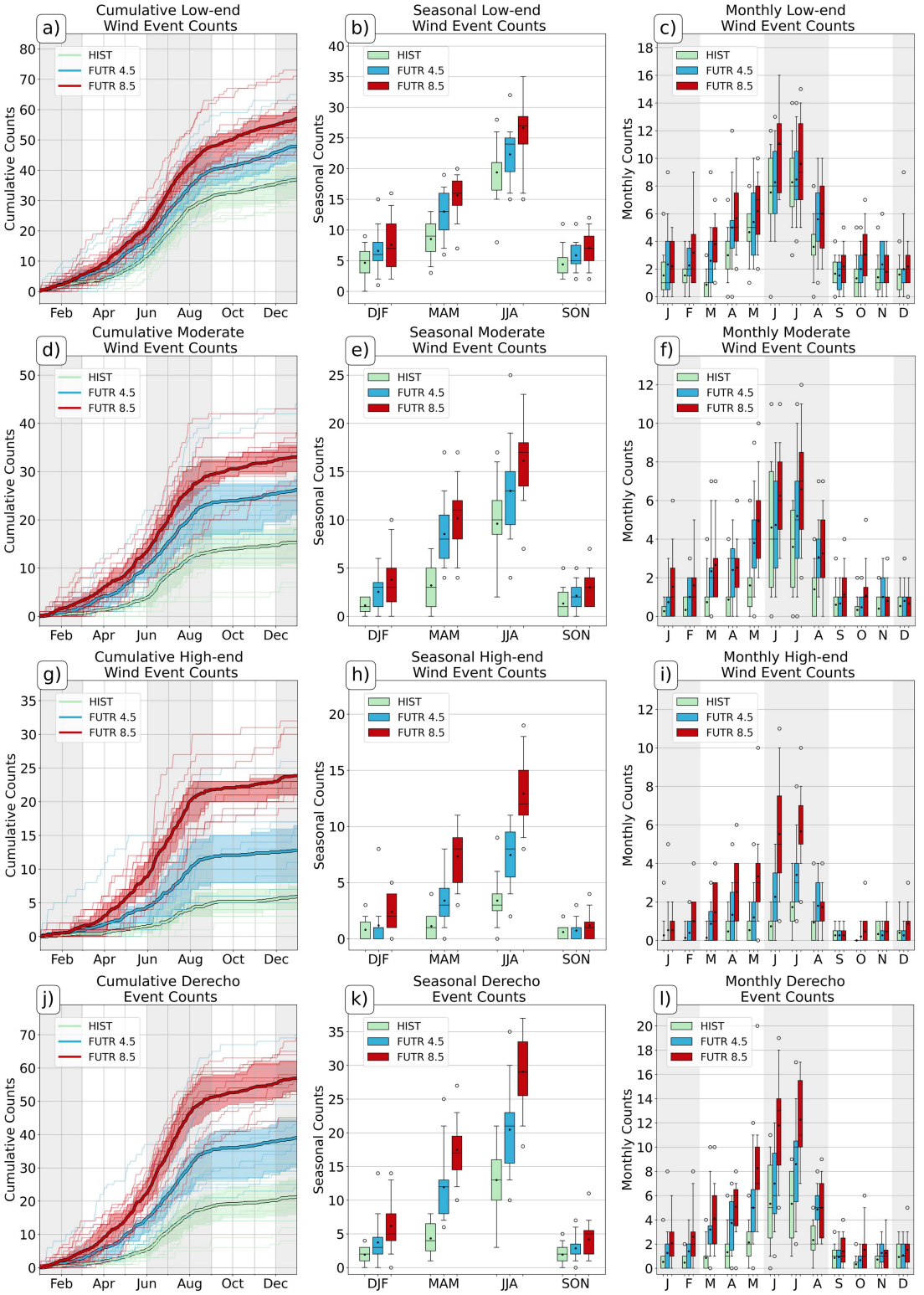

FIG. 3. Differences in (a),(d),(g) annual cumulative frequency counts, (b),(e),(h) seasonal counts, and (c),(f),(i) monthly counts for the CONUS for MCS swaths meeting (a)–(c) low-end, (d)–(f) moderate, (g)–(i) high-end, and (j)–(l) moderate + high-end, or derecho, criteria for the three epochs. In (a), (d), (g), and (j), means are denoted by thicker lines with the 25th- and 75th-percentile bounds provided in epoch-respective color shading. In (b), (c), (e), (f), (h), (i), (k), and (l), means are denoted by black dots, medians by black lines, interquartile range by boxes, 5th and 95th percentiles by whiskers, and outliers by clear circles.

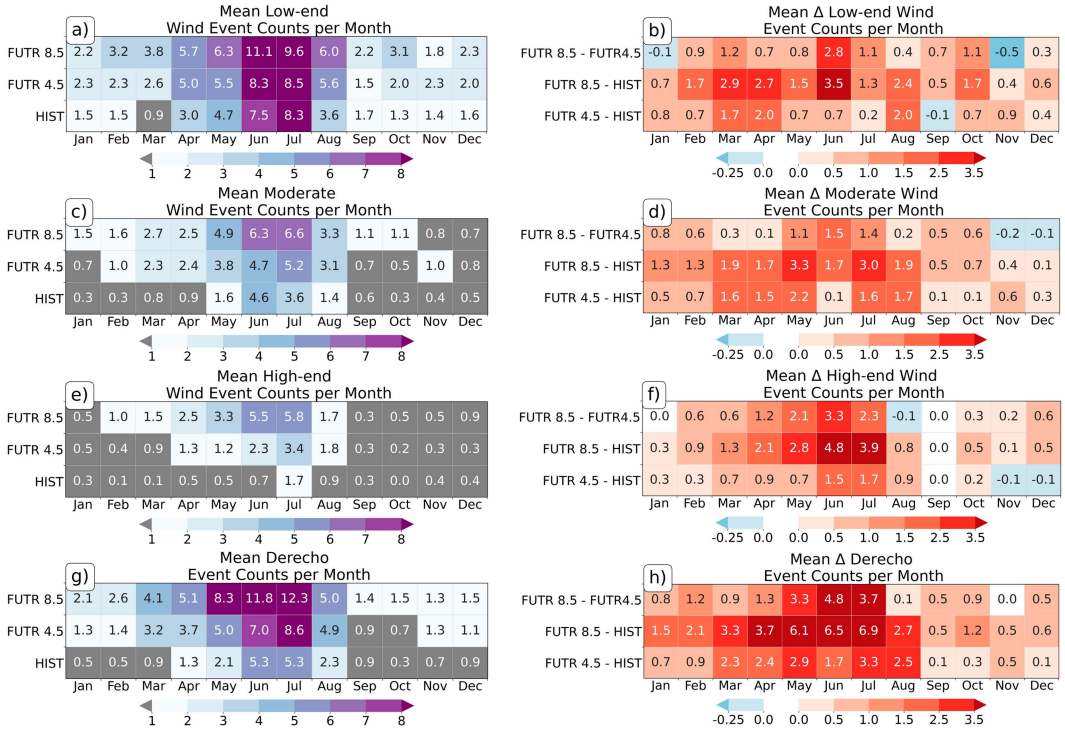

FIG. 4. Chiclets of the mean annual MCS swaths meeting (a) low-end, (c) moderate, (e) high-end, and (g) moderate + high-end, or derecho criteria per month for the three simulation epochs and the monthly count differences, or deltas, for MCS swaths meeting (b) low-end, (d) moderate, (f) high-end, and (h) moderate + high, or derecho, criteria between epochs labeled on *y* axis.

MCS swath populations are concentrated around maximized mean deltas, across a broad region extending from the Great Plains to the Ohio Valley FUTR epochs (Figs. 5e,f). Both FUTR 4.5 and 8.5 exhibit significant differences over the Ohio Valley during the warm season (Figs. 6e,f), but during the cool season, significant differences are concentrated across the southeast for FUTR 4.5 and slightly northward, over the Ark-La-Tex region extending into the Midwest, for FUTR 8.5 (Figs. 7e,f). Annually, mean (median) counts increase from 15.3 (16) events to 26.2 (27) events for FUTR 4.5 and 33.1 (34) events for FUTR 8.5 (Figs. 3d and 8d, Table 5, Table ES2), with significant changes observed outside the warm-season months (Figs. 3e,f and 4c,d, Fig. ES3b, Table ES2). The intensity of moderate MCS swaths is projected to increase for both future scenarios with significant changes in duration (Fig. 8e) and severe wind gust counts, especially in the spring season (Table ES2).

3) HIGH-END MCS SWATHS

Mean annual high-end MCS swath counts increase across northern and southern corridors (Figs. 5h,i), focused across the Midwest into the northeast during the warm season (Fig. 6h) and over the Ark-La-Tex region during the cool season for FUTR 4.5 (Fig. 7h). Similar, but more widespread, changes occur for FUTR 8.5 during the warm and cool seasons (Figs. 6i and 7i), with increased mean annual counts across the entire north–south extent between 100° and 80°W (Fig. 5i). Significant population differences are more evident for FUTR 8.5 for high-end MCS swaths across almost the entire eastern CONUS (Fig. 5i), driven by significant changes across this region in both the warm and cool seasons (Figs. 6i and 7i). High-end MCS swath counts more than double between epochs; mean (median) counts increase from 5.9 (5) events for HIST to 12.8 (13) events for FUTR 4.5 and 23.9 (23) events for FUTR 8.5 (Figs. 3g and 8g, Table 5, Table ES3), which are driven by significant increases during the spring and summer seasons under both future epochs (Figs. 3h,i and 4e,f, Fig. ES3c, Table ES3). Unlike low-end and moderate MCS swaths, hourly counts double or even triple for future scenarios (Fig. 9c).

Mean annual high-end MCS swath durations increase between epochs, and though increases in all other variables are observed, changes are only significant for FUTR 8.5 (Figs. 8h,i, Table 5, Table ES3). The FUTR 8.5 results are driven by significant changes on a consistent monthly basis for March through July for all variables, with the annual peak in high-end MCS swaths shifting from July to June and July in future epochs (Table ES3). This suggests that MCSs that produce high-end severe wind swaths, which often have characteristics of progressive derechos (Johns and Hirt 1987; Coniglio and Stensrud 2004; Guastini and Bosart 2016; Corfidi et al. 2016), are projected to be more frequent, longer-lived, and intense across both the spring and summer months.

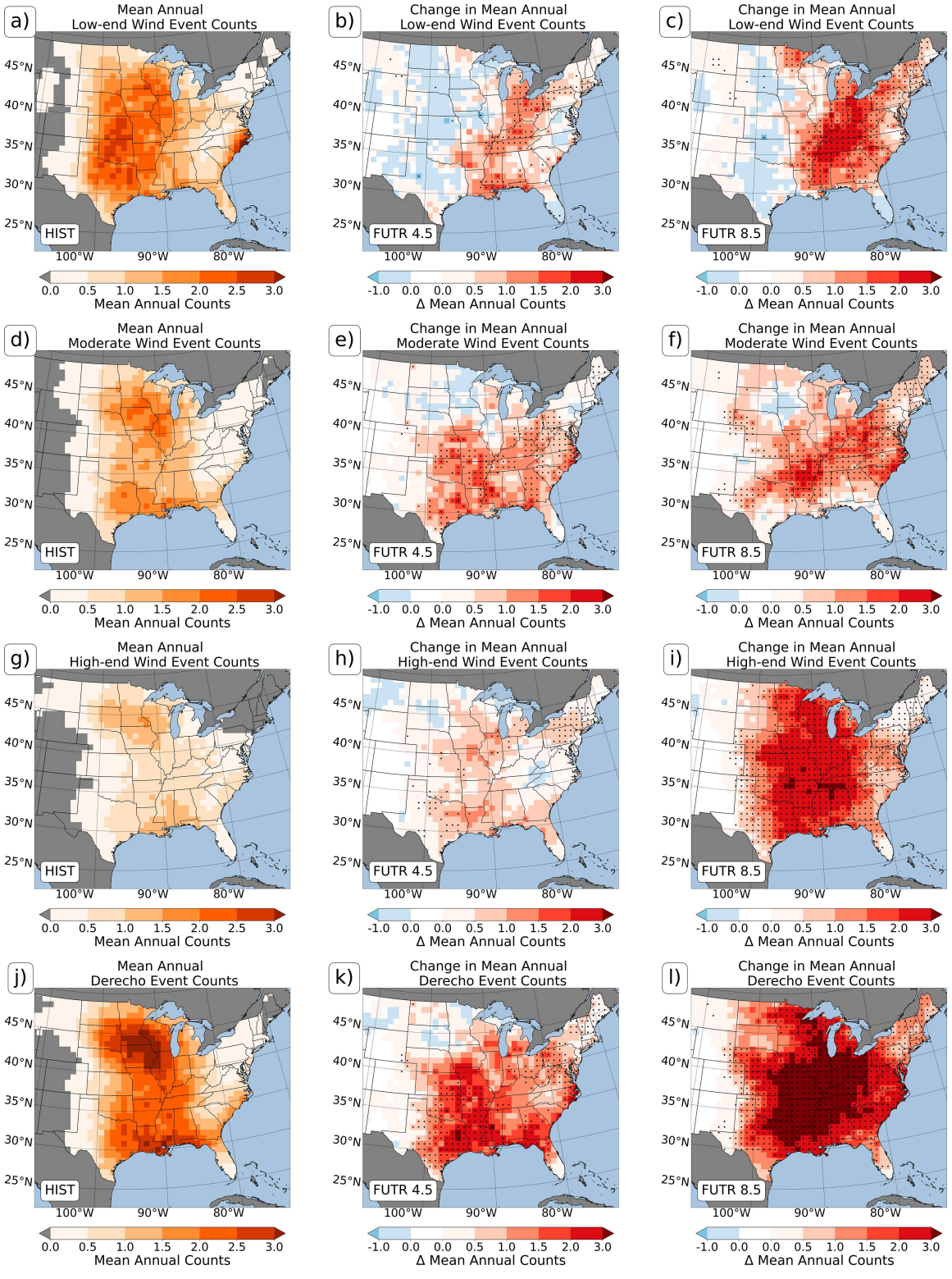

FIG. 5. Mean annual (a)–(c) low-end, (d)–(f) moderate, (g)–(i) high-end, and (j)–(l) moderate + high-end, or derecho, MCS swath counts on an 80-km grid. Mean annual counts are shown for (a),(d),(g),(j) HIST and for differences relative to HIST for (b),(e),(h),(k) FUTR 4.5 and (c),(f),(i),(l) FUTR 8.5. Stippling indicates a significant ($p < 0.05$; Mann–Whitney U test) difference between HIST and (b),(e),(h),(k) FUTR 4.5 and (c),(f),(i),(l) FUTR 8.5.

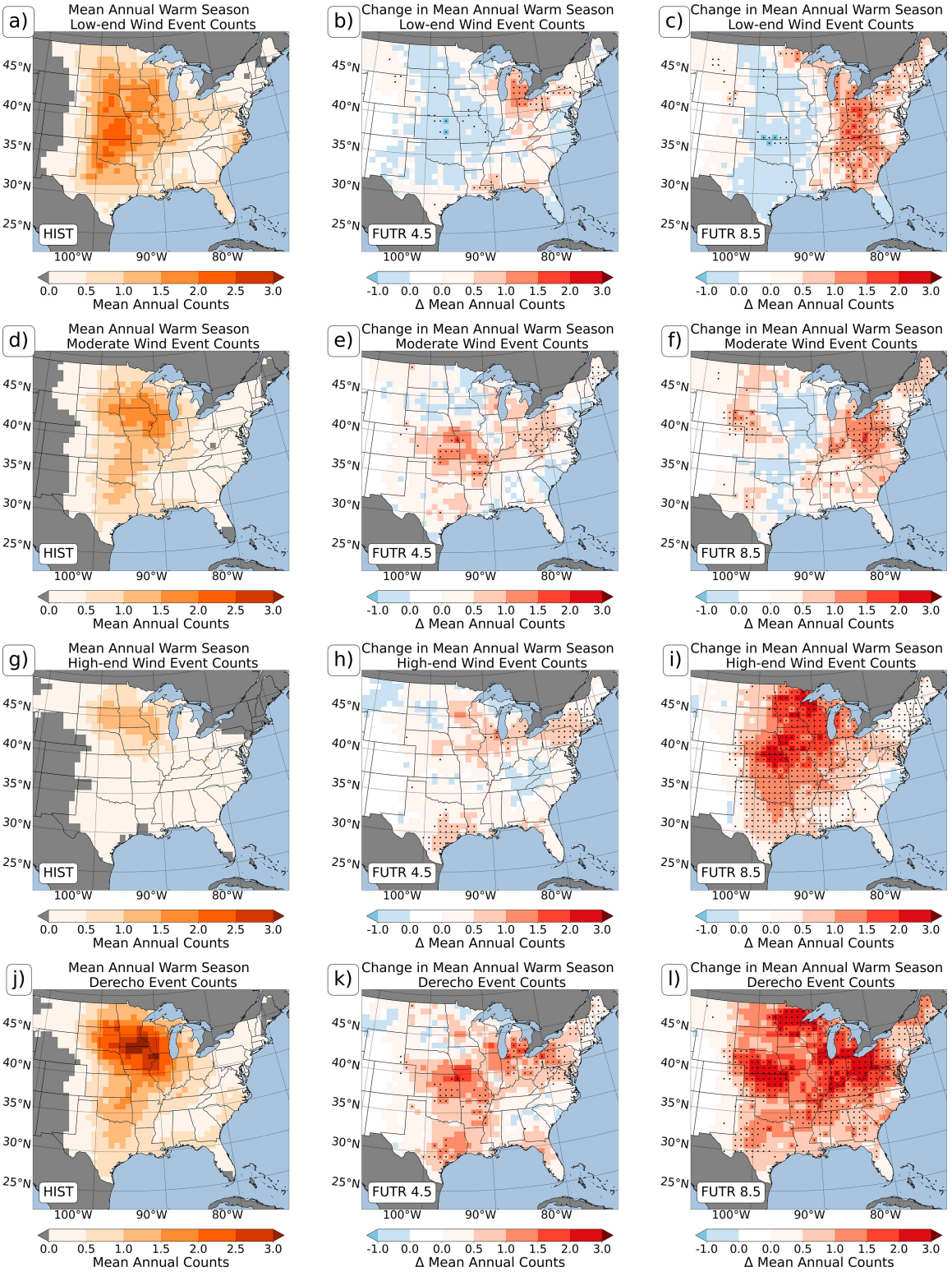

FIG. 6. As in Fig. 5, but for the mean annual warm season (May–August).

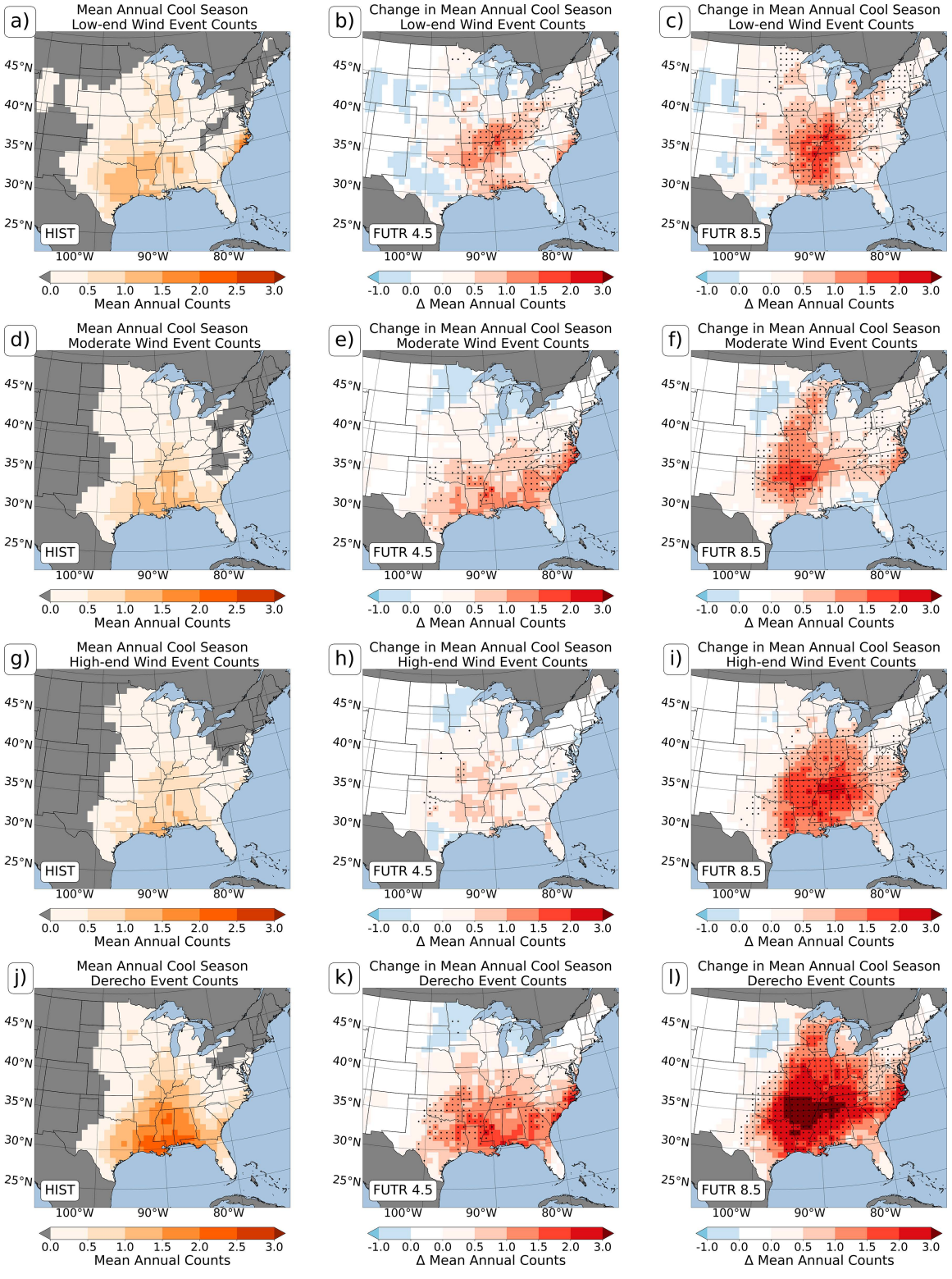

FIG. 7. As in Fig. 5, but for the mean annual cool season (September–April).

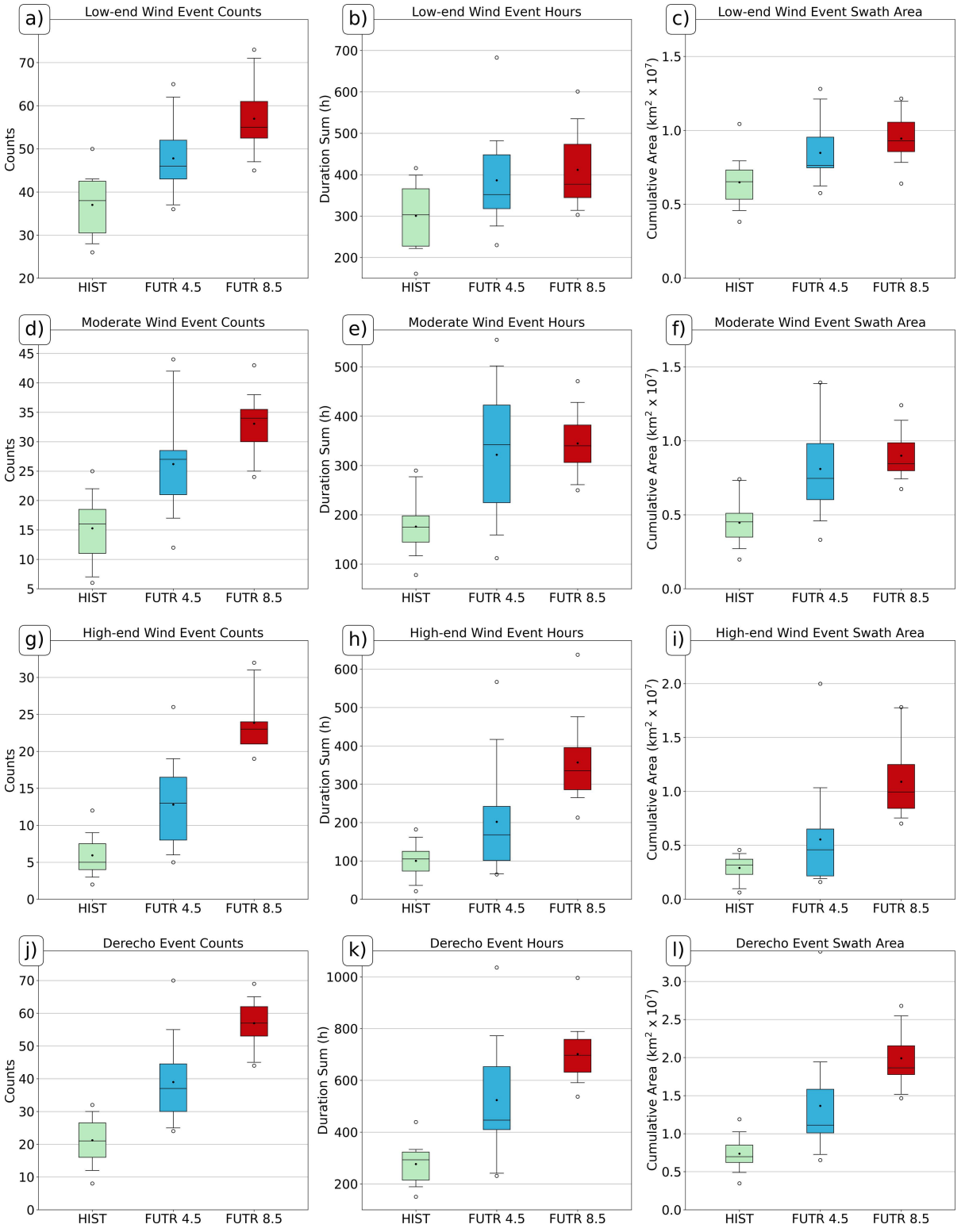

FIG. 8. Box-and-whisker plots illustrating annual CONUS (a)–(c) low-end, (d)–(f) moderate, (g)–(i) high-end, and (j)–(l) moderate + high, or derecho, MCS swath (a),(d),(g),(j) counts, (b),(e),(h),(k) sum of event hours, and (c),(f),(i),(l) wind swath area accumulation, or the total area of a wind swath attributed to an event. Box-and-whisker distributions and central tendencies are as in Fig. 3.

TABLE 5. Measures of central tendency for selected characteristics of low, moderate, high, and moderate + high, or derecho, MCS swaths for the CONUS. The count of gusts indicates the number of grid cells within an event-type wind swath experiencing a gust of the indicated threshold. All percent change values are positive.

	HIST	FUTR 4.5	FUTR 8.5	HIST v. FUTR 4.5	HIST v. FUTR 8.5		HIST	FUTR 4.5	FUTR 8.5	HIST v. FUTR 4.5	HIST v. FUTR 8.5
	Annual low-end wind events			% change			Annual moderate wind events			% change	
	Event count						Event count				
Mean	37.0	47.8	57.0	29.2	54.1	Mean	15.3	26.2	33.1	71.6	116.6
Median	38.0	46.0	55.0	21.1	44.7	Median	16.0	27.0	34.0	68.8	112.5
	Cumulative hours (h)						Cumulative hours (h)				
Mean	301.0	386.6	411.9	28.4	36.8	Mean	176.1	321.9	344.7	82.8	95.7
Median	303.0	352.0	377.0	16.2	24.4	Median	175.0	342.0	340.0	95.4	94.3
	Cumulative swath area ($km^2 \times 10^7$)						Cumulative swath area ($km^2 \times 10^7$)				
Mean	0.65	0.85	0.95	30.7	45.8	Mean	0.45	0.81	0.90	81.4	101.1
Median	0.65	0.76	0.93	16.9	42.5	Median	0.45	0.75	0.85	65.3	86.9
	Count of gusts $\geq$ 25.7 m s^{-1}						Count of gusts $\geq$ 25.7 m s^{-1}				
Mean	6840.9	7202.2	7236.6	5.3	5.8	Mean	8490.1	16 099.7	15 966.1	89.6	88.1
Median	6083.0	7229.0	6877.0	18.8	13.1	Median	8682.0	14 370.0	15 524.0	65.5	78.8
	Count of gusts $\geq$ 33.4 m s^{-1}						Count of gusts $\geq$ 33.4 m s^{-1}				
Mean	166.2	207.5	274.5	24.8	65.2	Mean	730.9	1362.1	1599.1	86.4	118.8
Median	134.0	196.0	266.0	46.3	98.5	Median	691.0	1279.0	1582.0	85.1	128.9
	Count of gusts $\geq$ 38 m s^{-1}						Count of gusts $\geq$ 38 m s^{-1}				
Mean	26.3	30.1	43.7	14.7	66.2	Mean	91.5	207.1	288.7	126.4	215.6
Median	14.0	21.0	29.0	50.0	107.1	Median	71.0	190.0	274.0	167.6	285.9
	Annual high end			% change			Annual derecho events			% change	
	Event count						Event count				
Mean	5.9	12.8	23.9	115.9	302.5	Mean	21.2	39.0	56.9	84.0	168.6
Median	5.0	13.0	23.0	160.0	360.0	Median	21.0	40.0	57.0	90.5	171.4
	Cumulative hours (h)						Cumulative hours (h)				
Mean	100.3	202.0	356.9	101.3	255.8	Mean	276.5	523.9	701.7	89.5	153.8
Median	105.0	168.0	335.0	60.0	219.0	Median	280.0	510.0	675.0	82.1	141.1
	Cumulative swath area ($km^2 \times 10^7$)						Cumulative swath area ($km^2 \times 10^7$)				
Mean	0.29	0.55	1.1	91.0	275.9	Mean	0.74	1.4	2.0	85.2	169.9
Median	0.32	0.46	0.99	44.8	213.2	Median	0.77	1.2	1.8	56.8	139.0
	Count of gusts $\geq$ 25.7 m s^{-1}						Count of gusts $\geq$ 25.7 m s^{-1}				
Mean	13 929.3	24 403.0	53 294.7	75.2	282.6	Mean	22 419.4	40 502.7	69 260.8	80.7	208.9
Median	9817.0	17 565.0	39 905.0	78.9	306.5	Median	18 499.0	31 935.0	55 429.0	72.6	199.6

TABLE 5. (*Continued*)

	HIST	FUTR 4.5	FUTR 8.5	HIST v. FUTR 4.5	HIST v. FUTR 8.5		HIST	FUTR 4.5	FUTR 8.5	HIST v. FUTR 4.5	HIST v. FUTR 8.5
Count of gusts ≥ 33.4 m s^{-1}						Count of gusts ≥ 33.4 m s^{-1}					
Mean	2619.6	4514.7	12 147.9	72.3	363.7	Mean	3350.5	5876.7	13 747.0	75.4	310.3
Median	2071.0	3697.0	9199.0	78.5	344.2	Median	2762.0	4976.0	10 781.0	80.2	290.3
Count of gusts ≥ 38 m s^{-1}						Count of gusts ≥ 38 m s^{-1}					
Mean	771.5	1254.0	4317.9	62.5	459.7	Mean	862.9	1461.1	4606.5	69.3	433.8
Median	549.0	1015.0	3374.0	84.9	514.6	Median	620.0	1205.0	3648.0	94.4	488.4

4) DERECHOS

Mean annual derecho counts increase across most of the eastern CONUS (Fig. 5k), especially for the FUTR 8.5 epoch, where positive deltas are maximized at an annual change in over three events per grid cell, the highest delta observed among all category types (Fig. 5l). Significant population differences are projected across the southern Great Plains and northeast for FUTR 4.5 (Fig. 5k) and most of the eastern CONUS for FUTR 8.5 (Fig. 5l). Warm-season derechos increase across a broad region north of 35°N extending from the central Great Plains to the Ohio Valley (Figs. 6k,l), while cool-season events increase across the southeast (Figs. 7k,l). Like high-end MCS swaths, significant seasonal population differences are more prevalent for FUTR 8.5 across the eastern CONUS (Figs. 6l and 7l). Mean (median) counts significantly increase from 21.2 (21) events in HIST to 39 (40) events in FUTR 4.5 and 56.9 (57) events in FUTR 8.5, corresponding to a near doubling and tripling of derechos, respectively, on an annual basis (Figs. 3j and 8j, Table 5, Table ES4). While derecho activity peaks in June and July across both the historical and future epochs, significant changes are projected for the spring and summer seasons for FUTR 4.5 and for all seasons for FUTR 8.5 (Figs. 3k,l and 4g,h, Fig. ES3d, Table ES4), suggesting they may be more likely outside the typical warm-season months, especially in the spring under future climates.

In addition to a longer season, changes in duration (Fig. 8k) and severe wind gust counts are significant on an annual basis for both future epochs, while wind swath area and other gust thresholds are only significant for FUTR 8.5 (Fig. 8l, Table ES4). Since derechos are composed of both moderate and high-end MCS swaths, it is no surprise that the intermediate scenario indicates significant changes in most characteristic variables for the spring and summer months and the pessimistic scenario suggests significant changes for the winter, spring, and summer months. These results suggest that, by the end of the twenty-first century, derechos could become not only more frequent, but longer-lived and capable of producing more severe wind gusts.

c. Environment discussion

The changes in derecho activity between the HIST and FUTR epochs could be due to corresponding shifts in fundamental ingredients, including shear and instability profiles, required for the initiation and sustenance of long-lived MCSs. Projected decreases in deep-layer (0–6 km) vertical wind shear, which enhances storm organization and longevity, specifically in the future pessimistic epoch (Ashley et al. 2023; their Figs. 7g–i), may not necessarily inhibit derecho activity across the eastern CONUS, as observed derechos have occurred in a wide range of shear environments (Evans and Doswell 2001; Coniglio et al. 2004, 2006, 2012; Ashley et al. 2007). Further, the importance of cold pool interactions with low-level (0–3 km), midlevel (3–6 km), and upper-level (>6 km) shear has been debated in the literature with regard to influence on strength and longevity of the parent MCS (Weisman and Rotunno 2004; Stensrud et al. 2005; Coniglio et al. 2006, 2012).

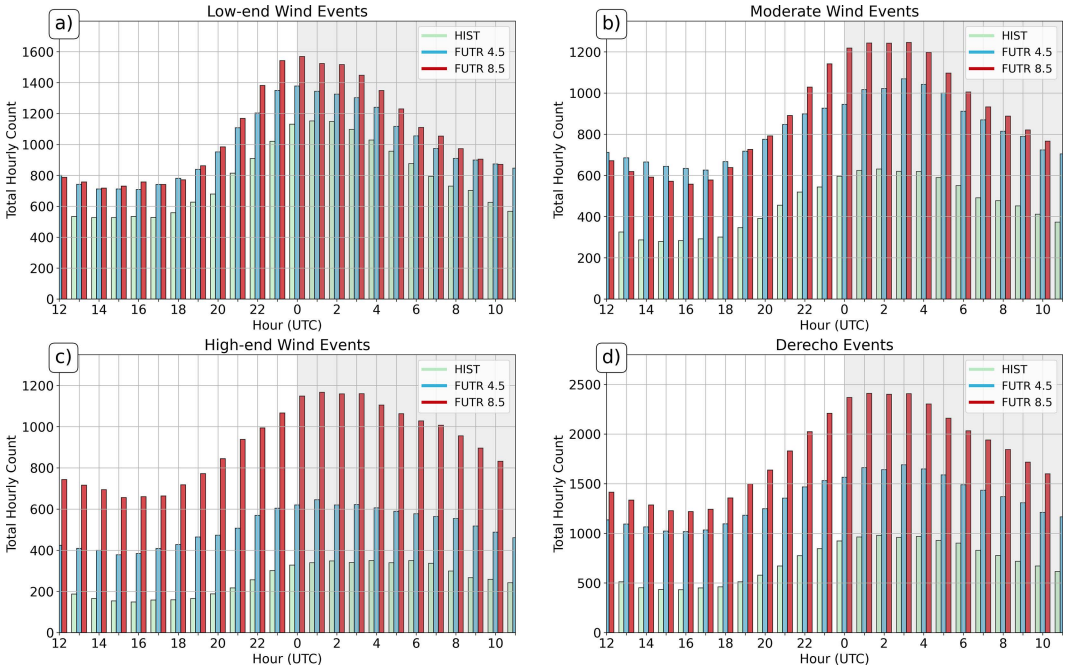

FIG. 9. Total hourly counts of (a) low-end, (b) moderate, (c) high-end, and (d) moderate + high, or derecho, MCS swaths for the three simulation epochs for the CONUS.

That said, even modest decreases in deep-layer flow can be offset by strong instability (Evans and Doswell 2001; Coniglio et al. 2004). Other climate change–focused studies have linked anthropogenic climate change to increases in instability, or CAPE, fueled by warmer temperatures and increased atmospheric moisture content, capable of supporting conditions that lead to thunderstorms and severe weather (Trapp et al. 2007, 2009; Diffenbaugh et al. 2013; Hoogewind et al. 2017; Haberlie et al. 2022; Ashley et al. 2023). Most unstable CAPE (MUCAPE) significantly increases throughout the east-central CONUS in the CP-RCM scenarios (Haberlie et al. 2022; their Fig. 4; Ashley et al. 2023; their Figs. 7a–c), which may help broadly explain increasing low-end, moderate, high-end, and derecho swath counts for both FUTR 4.5 and FUTR 8.5, particularly during the cool season across the mid-South (Haberlie et al. 2022; their Figs. 4a,b,d–f,j–l). Additionally, most unstable CIN (MUCIN) increases throughout the central CONUS, especially in the Great Plains during the warm season (Haberlie et al. 2022; their Fig. 4; Ashley et al. 2023; their Figs. 7d–f), which may be related to the decrease in low-end MCS swaths across the Great Plains in the warm season and the corresponding eastward shift (Figs. 6b,c) into potentially less capped environments where the process of underrunning—where a moist, unstable boundary layer air mass flows out from beneath the lid (Carlson et al. 1983; Farrell and Carlson 1989; Ashley et al. 2007)—is more likely to occur. Indeed, higher CIN values across the United States under projected future climates have been linked to decreases in storm development, especially in the Great Plains (Hoogewind et al. 2017; Rasmussen et al. 2020).

Projected spatiotemporal changes in shear, MUCAPE, and MUCIN can only broadly explain changes suggested between the HIST and FUTR epochs for low-end, moderate, high-end, and derecho MCS swath activity. Additional factors incorporated into the derecho composite parameter (Evans and Doswell 2001), which identifies environments conducive to cold pool-driven wind events, include downward CAPE (DCAPE) and ambient flow for cold pool generation and downstream development along the gust front. Although DCAPE was not assessed herein, the grid spacing employed by the CP-RCM has been found favorable for capturing simulated MCS cold pool intensity and propagation (Prein et al. 2021). Changes in other ingredients, like low-level moisture content, may lead to downstream profiles supportive of long-lived intense bow echoes since increases in moisture are expected under warming scenarios (Brooks 2013; Allen 2018), or may promote the development of isolated convection that could threaten cold pool dynamics (Li et al. 2023). Neighboring convection likely did impact longevity of MCS swaths in the CP-RCM simulations; however, this relationship is difficult to assess since shorter-lived events inhibited by isolated convection are likely not retained by the tracking and detection approach when Table 2 criteria are implemented. Additionally, potential changes in underlying forcing mechanisms (e.g., shortwave troughs, fronts associated with extratropical cyclones, and drylines) and favorable upper-level flow patterns (Coniglio et al. 2004; Ashley et al. 2007; Guastini and Bosart 2016) may lead to more favorable environments for derecho activity. While it is beyond the scope of this effort to investigate these additional considerations within the CP-RCM, future work should more thoroughly

evaluate these important ingredients, their overlap, and how changes in these environmental parameters may relate to changes in derecho and MCS windstorm populations.

The projected increases in derecho and other MCS-based windstorm activity suggested by this CP-RCM echo result from other works investigating SCS response to climate change (Brooks 2013; Diffenbaugh et al. 2013; Hoogewind et al. 2017; Rasmussen et al. 2020; Allen 2018; Lepore et al. 2021; Gensini 2021; Haberlie et al. 2022; Ashley et al. 2023) and align with findings that larger, more intense MCSs may be possible in future climates (Prein et al. 2017; Haberlie et al. 2024). However, as computing and storage resources expand, additional concerted efforts are necessary. Multiple ensembles, different microphysics and parameterization schemes, various RCP scenarios, and both implicit and explicit analyses should be conducted to comprehensively investigate the impact of anthropogenic climate change on CONUS derecho activity.

5. Conclusions

The relationship between derechos and anthropogenic climate change has received little attention in the literature (González-Alemán et al. 2023; Li et al. 2023; Lasher-Trapp et al. 2023) compared to other forms of SCSs (compare Trapp and Hoogewind 2016; Hoogewind et al. 2017; Trapp et al. 2019; Gensini 2021; Haberlie et al. 2022, 2023; Ashley et al. 2023) despite their significant, and often widespread, societal impacts (Ashley and Mote 2005; Squitieri et al. 2023a). Here, a modified version of an MCS identification and tracking algorithm (Haberlie and Ashley 2018a,b) and derecho criteria derived from Fujita and Wakimoto (1981), Johns and Hirt (1987), and Coniglio and Stensrud (2004) are applied to high-resolution, dynamically downscaled climate simulation output. This explicit approach assessed how the climatology of CONUS derechos, and other MCS-based windstorms, may change during the twenty-first century under two different greenhouse gas emission trajectories.

Results reveal that MCS-based windstorm activity, including derechos, could increase across most portions of the eastern CONUS and is projected to become more common during the spring and summer months, with the largest positive deltas observed for the pessimistic end-of-the-century scenario. The highlights of spatiotemporal changes include the following:

- Low-end MCS swaths may become more prevalent across all seasons, particularly the spring months, in the mid-South and Appalachia. Decreases observed in the future epochs across the Great Plains are likely explained by increased inhibition suppressing MCS development during the warm season in this region.
- Moderate MCS swaths may become more common year-round across most of the eastern CONUS, especially in the future pessimistic scenario.
- High-end MCS swaths may become more common and more intense in the spring and summer seasons across the southern Great Plains and the Midwest, with notable increases observed in a future pessimistic climate.
- Derechos could become more frequent, with mean annual counts nearly doubling (intermediate scenario) and tripling (pessimistic scenario) by the end of the twenty-first century in some regions, and may be longer-lived, more expansive, and capable of producing more damaging wind gusts across large portions of the central and eastern CONUS.

While this study assesses spatiotemporal shifts in derecho populations, changes are broadly explained by regional migration of favorable tropospheric kinematics and thermodynamics. Further implicit and explicit research should aim to assess derecho-specific environments (Evans and Doswell 2001; Coniglio et al. 2004; Guastini and Bosart 2016), as well as spatiotemporal changes in important drivers of derecho activity: QLCSs and extratropical cyclone activity. Further, as data storage and computational abilities increase, more severe wind gust proxies such as 2- and 80-m wind should be evaluated to investigate not only potential changes in MCS-based windstorm activity but also severe convective wind.

This study only provides an initial set of perspectives on future derecho potential during the twenty-first century based on 15-yr CP-RCM simulations, one GCM, and one set of model parameters. Other studies leveraging climate model output to discuss changes in convective populations stress the importance of future research encompassing additional GCMs, longer simulation periods, ensemble modeling approaches in both implicit and explicit frameworks, alternative emissions/climate projections, and use of multiple microphysics and parameterization schemes (Gensini 2021; Ashley et al. 2023; Haberlie et al. 2023). These efforts would not only assist in communicating the spectrum of possibilities for derechos in a warning climate but may also lead to an improved understanding of model sensitivity and uncertainty associated with the use of different GCMs and model configurations. The results of this study, along with many others investigating SCSs in a changing climate, support and stress the importance of efforts to mitigate, adapt to, and become resilient against wind-related perils should rising emissions continue.

Acknowledgments. This research was supported by the National Science Foundation Awards 1637225 and 1800582 and the National Oceanic and Atmospheric Administration Award NA22OAR4690645. The authors acknowledge high-performance computing support from Cheyenne (https://doi.org/10.5065/D6RX99HX) provided by NCAR's Computational and Information Systems Laboratory, sponsored by the National Science Foundation. We also acknowledge and thank Dr. Michael Papka (ANL) for data storage and post-processing assistance. This research used resources of the Argonne Leadership Computing Facility, which is a DOE Office of Science User Facility supported under Contract DE-AC02-06CH11357. We thank the reviewers for their constructive comments and suggestions.

Data availability statement. In the spirit of reproducibility, if an email request is made to the authors, we will make

available data and materials necessary to interested researchers for duplication and verification of results herein. WRF-BCC simulation output is available in netCDF format and stored on NCAR and/or Argonne systems. We request that anyone interested in using the WRF-BCC output contact coauthor Gensini (vgensini@niu.edu) for information on how to access the data, including any collaboration.

REFERENCES

Adams-Selin, R. D., S. C. van den Heever, and R. H. Johnson, 2013: Sensitivity of bow-echo simulation to microphysical parameterizations. *Wea. Forecasting*, **28**, 1188–1209, https://doi.org/10.1175/WAF-D-12-00108.1.

Allen, J. T., 2018: Climate change and severe thunderstorms. *Oxford Research Encyclopedia of Climate Science*, H. Brooks Ed., Oxford University Press, 67 pp., https://doi.org/10.1093/acrefore/9780190228620.013.62.

Ashley, W. S., and T. L. Mote, 2005: Derecho hazards in the United States. *Bull. Amer. Meteor. Soc.*, **86**, 1577–1592, https://doi.org/10.1175/BAMS-86-11-1577.

——, and S. M. Strader, 2016: Recipe for disaster: How the dynamic ingredients of risk and exposure are changing the tornado disaster landscape. *Bull. Amer. Meteor. Soc.*, **97**, 767–786, https://doi.org/10.1175/BAMS-D-15-00150.1.

——, T. L. Mote, and M. L. Bentley, 2005: On the episodic nature of derecho-producing convective systems in the United States. *Int. J. Climatol.*, **25**, 1915–1932, https://doi.org/10.1002/joc.1229.

——, ——, and ——, 2007: The extensive episode of derecho-producing convective systems in the United States during May and June 1998: A multi-scale analysis and review. *Meteor. Appl.*, **14**, 227–244, https://doi.org/10.1002/met.23.

——, S. Strader, T. Rosencrants, and A. J. Krmenec, 2014: Spatio-temporal changes in tornado hazard exposure: The case of the expanding bull's-eye effect in Chicago, Illinois. *Wea. Climate Soc.*, **6**, 175–193, https://doi.org/10.1175/WCAS-D-13-00047.1.

——, A. M. Haberlie, and J. Strohm, 2019: A climatology of quasi-linear convective systems and their hazards in the United States. *Wea. Forecasting*, **34**, 1605–1631, https://doi.org/10.1175/WAF-D-19-0014.1.

——, ——, and V. A. Gensini, 2023: The future of supercells in the United States. *Bull. Amer. Meteor. Soc.*, **104**, E1–E21, https://doi.org/10.1175/BAMS-D-22-0027.1.

Bengtsson, L., K. I. Hodges, and E. Roeckner, 2006: Storm tracks and climate change. *J. Climate*, **19**, 3518–3543, https://doi.org/10.1175/JCLI3815.1.

Bentley, M. L., and T. L. Mote, 1998: A climatology of derecho-producing mesoscale convective systems in the central and eastern United States, 1986–95. Part I: Temporal and spatial distribution. *Bull. Amer. Meteor. Soc.*, **79**, 2527–2540, https://doi.org/10.1175/1520-0477(1998)079<2527:ACODPM>2.0.CO;2.

——, and ——, 2000: A reply to comments on "A climatology of derecho producing mesoscale convective systems 1986–95. Part I: Temporal and spatial distribution." *Bull. Amer. Meteor. Soc.*, **81**, 1054–1057, https://doi.org/10.1175/1520-0477(2000)081<1054:REPLY>2.3.CO;2.

——, and A. J. Sparks, 2003: A 15 yr climatology of derecho-producing mesoscale convective systems over the central and eastern United States. *Climate Res.*, **24**, 129–139, https://doi.org/10.3354/cr024129.

Brooks, H. E., 2013: Severe thunderstorms and climate change. *Atmos. Res.*, **123**, 129–138, https://doi.org/10.1016/j.atmosres.2012.04.002.

Bruyère, C. L., J. M. Done, G. J. Holland, and S. Fredrick, 2014: Bias corrections of global models for regional climate simulations of high-impact weather. *Climate Dyn.*, **43**, 1847–1856, https://doi.org/10.1007/s00382-013-2011-6.

——, A. J. Monaghan, D. F. Steinhoff, and D. Yates, 2015: Bias-corrected CMIP5 CESM data in WRF/MPAS intermediate file format. NCAR Tech. Note NCAR/TN-515+STR, 27 pp., https://doi.org/10.5065/D6445JJ7.

Bundy, L. R., V. A. Gensini, and M. S. Russo, 2022: Insured corn losses in the United States from weather and climate Perils. *J. Appl. Meteor. Climatol.*, **61**, 969–988, https://doi.org/10.1175/JAMC-D-21-0245.1.

Burke, P. C., and D. M. Schultz, 2004: A 4-Yr climatology of cold-season bow echoes over the continental United States. *Wea. Forecasting*, **19**, 1061–1074, https://doi.org/10.1175/811.1.

Carlson, T. N., S. G. Benjamin, G. S. Forbes, and Y.-F. Li, 1983: Elevated mixed layers in the regional severe storm environment: Conceptual model and case studies. *Mon. Wea. Rev.*, **111**, 1453–1474, https://doi.org/10.1175/1520-0493(1983)111<1453:EMLITR>2.0.CO;2.

Cheeks, S. M., S. Fueglistaler, and S. T. Garner, 2020: A satellite-based climatology of central and southeastern U.S. mesoscale convective systems. *Mon. Wea. Rev.*, **148**, 2607–2621, https://doi.org/10.1175/MWR-D-20-0027.1.

Christensen, J. H., F. Boberg, O. B. Christensen, and P. Lucas-Picher, 2008: On the need for bias correction of regional climate change projections of temperature and precipitation. *Geophys. Res. Lett.*, **35**, L20709, https://doi.org/10.1029/2008GL035694.

Coniglio, M. C., and D. J. Stensrud, 2004: Interpreting the climatology of derechos. *Wea. Forecasting*, **19**, 595–605, https://doi.org/10.1175/1520-0434(2004)019<0595:ITCOD>2.0.CO;2.

——, ——, and M. B. Richman, 2004: An observational study of derecho-producing convective systems. *Wea. Forecasting*, **19**, 320–337, https://doi.org/10.1175/1520-0434(2004)019<0320:AOSODC>2.0.CO;2.

——, ——, and L. J. Wicker, 2006: Effects of upper-level shear on the structure and maintenance of strong quasi-linear mesoscale convective systems. *J. Atmos. Sci.*, **63**, 1231–1252, https://doi.org/10.1175/JAS3681.1.

——, S. F. Corfidi, and J. S. Kain, 2012: Views on applying RKW theory: An illustration using the 8 May 2009 derecho-producing convective system. *Mon. Wea. Rev.*, **140**, 1023–1043, https://doi.org/10.1175/MWR-D-11-00026.1.

Corfidi, S. F., M. C. Coniglio, A. E. Cohen, and C. M. Mead, 2016: A proposed revision to the definition of "derecho". *Bull. Amer. Meteor. Soc.*, **97**, 935–949, https://doi.org/10.1175/BAMS-D-14-00254.1.

Creighton, G., E. Kuchera, R. Adams-Selin, J. McCormick, S. Rentschler, and B. Wickard, 2014: AFWA diagnostics in WRF. 17 pp., https://citeseerx.ist.psu.edu/document?repid=rep1&type=pdf&doi=5b4876dc88613a9cf49ec6c33f35317b01c63232.

Cui, W., X. Dong, B. Xi, and Z. Feng, 2021: Climatology of linear mesoscale convective system morphology in the United States based on the random-forests method. *J. Climate*, **34**, 7257–7276, https://doi.org/10.1175/JCLI-D-20-0862.1.

Daly, C., R. P. Neilson, and D. L. Phillips, 1994: A statistical-topographic model for mapping climatological precipitation over mountainous Terrain. *J. Appl. Meteor.*, **33**, 140–158,

https://doi.org/10.1175/1520-0450(1994)033<0140:ASTMFM>2.0.CO;2.

Dee, D. P., and Coauthors, 2011: The ERA-Interim reanalysis: Configuration and performance of the data assimilation system. *Quart. J. Roy. Meteor. Soc.*, **137**, 553–597, https://doi.org/10.1002/qj.828.

Diffenbaugh, N. S., M. Scherer, and R. J. Trapp, 2013: Robust increases in severe thunderstorm environments in response to greenhouse forcing. *Proc. Natl. Acad. Sci. USA*, **110**, 16 361–16 366, https://doi.org/10.1073/pnas.1307758110.

Doswell, C. A., III, H. E. Brooks, and M. P. Kay, 2005: Climatological estimates of daily local nontornadic severe thunderstorm probability for the United States. *Wea. Forecasting*, **20**, 577–595, https://doi.org/10.1175/WAF866.1.

Edwards, R., J. T. Allen, and G. W. Carbin, 2018: Reliability and climatological impacts of convective wind estimations. *J. Appl. Meteor. Climatol.*, **57**, 1825–1845, https://doi.org/10.1175/JAMC-D-17-0306.1.

Evans, J. S., and C. A. Doswell III, 2001: Examination of derecho environments using proximity soundings. *Wea. Forecasting*, **16**, 329–342, https://doi.org/10.1175/1520-0434(2001)016<0329:EODEUP>2.0.CO;2.

Farrell, R. J., and T. N. Carlson, 1989: Evidence for the role of the lid and underrunning in an outbreak of tornadic thunderstorms. *Mon. Wea. Rev.*, **117**, 857–871, https://doi.org/10.1175/1520-0493(1989)117<0857:EFTROT>2.0.CO;2.

Feng, Z., and Coauthors, 2021: A global high-resolution mesoscale convective system database using satellite-derived cloud tops, surface precipitation, and tracking. *J. Geophys. Res. Atmos.*, **126**, e2020JD034202, https://doi.org/10.1029/2020JD034202.

Figurski, M. J., G. Nykiel, A. Jaczewski, Z. Baldysz, and M. Wdowikowski, 2022: The impact of initial and boundary conditions on severe weather event simulations using a high-resolution WRF model. Case study of the derecho event in Poland on 11 August 2017. *Meteor. Hydrol. Water Manage.*, **10**, 60–87, https://doi.org/10.26491/mhwm/143877.

Fritzen, R., V. Lang, and V. A. Gensini, 2021: Trends and variability of North American cool-season extratropical cyclones: 1979–2019. *J. Appl. Meteor. Climatol.*, **60**, 1319–1331, https://doi.org/10.1175/JAMC-D-20-0276.1.

Fujita, T. T., and R. M. Wakimoto, 1981: Five scales of airflow associated with a series of downbursts on 16 July 1980. *Mon. Wea. Rev.*, **109**, 1438–1456, https://doi.org/10.1175/1520-0493(1981)109<1438:FSOAAW>2.0.CO;2.

Gensini, V. A., 2021: Severe convective storms in a changing climate. *Climate Change and Extreme Events*, A. Fares, Ed., Springer, 39–56, https://doi.org/10.1016/B978-0-12-822700-8.00007-X.

——, and T. L. Mote, 2014: Estimations of hazardous convective weather in the United States using dynamical downscaling. *J. Climate*, **27**, 6581–6589, https://doi.org/10.1175/JCLI-D-13-00777.1.

——, and ——, 2015: Downscaled estimates of late 21st century severe weather from CCSM3. *Climatic Change*, **129**, 307–321, https://doi.org/10.1007/s10584-014-1320-z.

——, C. Ramseyer, and T. L. Mote, 2014: Future convective environments using NARCCAP. *Int. J. Climatol.*, **34**, 1699–1705, https://doi.org/10.1002/joc.3769.

——, A. M. Haberlie, and W. S. Ashley, 2023: Convection-permitting simulations of historical and possible future climate over the contiguous United States. *Climate Dyn.*, **60**, 109–126, https://doi.org/10.1007/s00382-022-06306-0.

González-Alemán, J. J., D. Insua-Costa, E. Bazile, S. González-Herrero, M. Marcello Miglietta, P. Groenemeijer, and M. G. Donat, 2023: Anthropogenic warming had a crucial role in triggering the historic and destructive Mediterranean derecho in summer 2022. *Bull. Amer. Meteor. Soc.*, **104**, E1526–E1532, https://doi.org/10.1175/BAMS-D-23-0119.1.

Guastini, C. T., and L. F. Bosart, 2016: Analysis of a progressive derecho climatology and associated formation environments. *Mon. Wea. Rev.*, **144**, 1363–1382, https://doi.org/10.1175/MWR-D-15-0256.1.

Haberlie, A. M., and W. S. Ashley, 2018a: A method for identifying midlatitude mesoscale convective systems in radar mosaics. Part I: Segmentation and classification. *J. Appl. Meteor. Climatol.*, **57**, 1575–1598, https://doi.org/10.1175/JAMC-D-17-0293.1.

——, and ——, 2018b: A method for identifying midlatitude mesoscale convective systems in radar mosaics. Part II: Tracking. *J. Appl. Meteor. Climatol.*, **57**, 1599–1621, https://doi.org/10.1175/JAMC-D-17-0294.1.

——, and ——, 2019a: A radar-based climatology of mesoscale convective systems in the United States. *J. Climate*, **32**, 1591–1606, https://doi.org/10.1175/JCLI-D-18-0559.1.

——, and ——, 2019b: Climatological representation of mesoscale convective systems in a dynamically downscaled climate simulation. *Int. J. Climatol.*, **39**, 1144–1153, https://doi.org/10.1002/joc.5880.

——, ——, C. M. Battisto, and V. A. Gensini, 2022: Thunderstorm activity under intermediate and extreme climate change scenarios. *Geophys. Res. Lett.*, **49**, e2022GL098779, https://doi.org/10.1029/2022GL098779.

——, ——, V. A. Gensini, and A. C. Michaelis, 2023: The ratio of mesoscale convective system precipitation to total precipitation increases in future climate change scenarios. *npj Climate Atmos. Sci.*, **6**, 150, https://doi.org/10.1038/s41612-023-00481-5.

——, B. Wallace, W. S. Ashley, V. Gensini, and A. Michaelis, 2024: Mesoscale convective system activity in the United States under intermediate and extreme climate change scenarios. *Climatic Change*, **177**, 94, https://doi.org/10.1007/s10584-024-03752-z.

Harper, B. A., J. D. Kepert, and J. D. Ginger, 2010: Guidelines for converting between various wind averaging periods in tropical cyclone conditions. WMO Tech. Doc. WMO/TD-1555, 64 pp., https://www.systemsengineeringaustralia.com.au/download/WMO_TC_Wind_Averaging_27_Aug_2010.pdf.

Harris, A. R., and J. D. W. Kahl, 2017: Gust factors: Meteorologically stratified climatology, data artifacts, and utility in forecasting peak gusts. *J. Appl. Meteor. Climatol.*, **56**, 3151–3166, https://doi.org/10.1175/JAMC-D-17-0133.1.

Hinrichs, G. D., 1888: Tornadoes and derechos. *Amer. Meteor. J.*, **5**, 341–349.

Hoogewind, K. A., M. E. Baldwin, and R. J. Trapp, 2017: The impact of climate change on hazardous convective weather in the United States: Insight from high-resolution dynamical downscaling. *J. Climate*, **30**, 10 081–10 100, https://doi.org/10.1175/JCLI-D-16-0885.1.

Houze, R. A., Jr., 2004: Mesoscale convective systems. *Rev. Geophys.*, **42**, RG4003, https://doi.org/10.1029/2004RG000150.

——, 2018: 100 years of research on mesoscale convective systems. *A Century of Progress in Atmospheric and Related Sciences: Celebrating the American Meteorological Society Centennial*, *Meteor. Monogr.*, No. 59, Amer. Meteor. Soc., https://doi.org/10.1175/AMSMONOGRAPHS-D-18-00s01.1.

IPCC, 2021: *Climate Change 2021: The Physical Science Basis*. V. Masson-Delmotte et al., Eds., Cambridge University Press, 2409 pp., www.ipcc.ch/report/ar6/wg1/.

Johns, R. H., and W. D. Hirt, 1987: Derechos: Widespread convectively induced windstorms. *Wea. Forecasting*, **2**, 32–49, https://doi.org/10.1175/1520-0434(1987)002<0032:DWCIW>2.0.CO;2.

——, and J. S. Evans, 2000: Comments on "A climatology of derecho-producing mesoscale convective systems in the central and eastern United States, 1986–95. Part I: Temporal and spatial distribution". *Bull. Amer. Meteor. Soc.*, **81**, 1049–1054, https://doi.org/10.1175/1520-0477(2000)081<1049:COACOD>2.3.CO;2.

Jung, C., L. Demant, P. Meyer, and D. Schindler, 2022: Highly resolved modeling of extreme wind speed in North America and Europe. *Atmos. Sci. Lett.*, **23**, e1082, https://doi.org/10.1002/asl.1082.

Kendon, E. J., A. F. Prein, C. A. Senior, and A. Stirling, 2021: Challenges and outlook for convection-permitting climate modelling. *Philos. Trans. Roy. Soc.*, **A379**, 20190547, https://doi.org/10.1098/rsta.2019.0547.

Kunkel, K. E., and Coauthors, 2013: Monitoring and understanding trends in extreme storms: State of knowledge. *Bull. Amer. Meteor. Soc.*, **94**, 499–514, https://doi.org/10.1175/BAMS-D-11-00262.1.

Lakshmanan, V., and T. Smith, 2009: Data mining storm attributes from spatial grids. *J. Atmos. Oceanic Technol.*, **26**, 2353–2365, https://doi.org/10.1175/2009JTECHA1257.1.

——, and ——, 2010: An objective method of evaluating and devising storm-tracking algorithms. *Wea. Forecasting*, **25**, 701–709, https://doi.org/10.1175/2009WAF2222330.1.

Lang, V. A., T. J. Turner, B. R. Selbig, A. R. Harris, and J. D. W. Kahl, 2022: Predicting peak wind gusts during specific weather types with the meteorologically stratified gust factor model. *Wea. Forecasting*, **37**, 1435–1446, https://doi.org/10.1175/WAF-D-21-0201.1.

Lasher-Trapp, S., S. A. Orendorf, and R. J. Trapp, 2023: Investigating a derecho in a future warmer climate. *Bull. Amer. Meteor. Soc.*, **104**, E1831–E1852, https://doi.org/10.1175/BAMS-D-22-0173.1.

Lepore, C., R. Abernathey, N. Henderson, J. T. Allen, and M. K. Tippett, 2021: Future global convective environments in CMIP6 models. *Earth's Future*, **9**, e2021EF002277, https://doi.org/10.1029/2021EF002277.

Li, J., Y. Qian, L. R. Leung, X. Chen, Z. Yang, and Z. Feng, 2023: Potential weakening of the June 2012 North American derecho under future warming conditions. *J. Geophys. Res. Atmos.*, **128**, e2022JD037494, https://doi.org/10.1029/2022JD037494.

Liu, C., and Coauthors, 2016: Continental-scale convection-permitting modeling of the current and future climate of North America. *Climate Dyn.*, **49**, 71–95, https://doi.org/10.1007/s00382-016-3327-9.

Liu, W., P. A. Ullrich, J. Li, C. Zarzycki, P. M. Caldwell, L. R. Leung, and Y. Qian, 2023: The June 2012 North American derecho: A testbed for evaluating regional and global climate modeling systems at cloud-resolving scales. *J. Adv. Model. Earth Syst.*, **15**, e2022MS003358, https://doi.org/10.1029/2022MS003358.

Lucas-Picher, P., D. Argüeso, E. Brisson, Y. Tramblay, P. Berg, A. Lemonsu, S. Kotlarski, and C. Caillaud, 2021: Convection-permitting modeling with regional climate models: Latest developments and next steps. *Wiley Interdiscip. Rev.: Climate Change*, **12**, e731, https://doi.org/10.1002/wcc.731.

Marsh, P. T., H. E. Brooks, and D. J. Karoly, 2007: Assessment of the severe weather environment in North America simulated by a global climate model. *Atmos. Sci. Lett.*, **8**, 100–106, https://doi.org/10.1002/asl.159.

Miguez-Macho, G., G. L. Stenchikov, and A. Robock, 2004: Spectral nudging to eliminate the effects of domain position and geometry in regional climate model simulations. *J. Geophys. Res.*, **109**, D13104, https://doi.org/10.1029/2003JD004495.

Milne, J. M., 2016: Verification of 10-meter wind forecasts from NSSL-WRF in predicting severe wind-producing MCSs. M.S. thesis, Dept. of Geography and Environmental Sustainability, The University of Oklahoma, 77 pp., https://shareok.org/bitstream/handle/11244/47072/2016_Milne_Jeffrey_Thesis.pdf?sequence=1&isAllowed=y.

NOAA NCEI, 2023: U.S. billion-dollar weather and climate disasters, https://doi.org/10.25921/stkw-7w73.

Núñez Ocasio, K. M., J. L. Evans, and G. S. Young, 2020: Tracking mesoscale convective systems that are potential candidates for tropical cyclogenesis. *Mon. Wea. Rev.*, **148**, 655–669, https://doi.org/10.1175/MWR-D-19-0070.1.

Parker, M. D., and R. H. Johnson, 2000: Organizational modes of midlatitude mesoscale convective systems. *Mon. Wea. Rev.*, **128**, 3413–3436, https://doi.org/10.1175/1520-0493(2001)129<3413:OMOMMC>2.0.CO;2.

Prein, A. F., 2023: Thunderstorm straight line winds intensify with climate change. *Nat. Climate Change*, **13**, 1353–1359, https://doi.org/10.1038/s41558-023-01852-9.

——, and Coauthors, 2015: A review on regional convection-permitting climate modeling: Demonstrations, prospects, and challenges. *Rev. Geophys.*, **53**, 323–361, https://doi.org/10.1002/2014RG000475.

——, C. Liu, K. Ikeda, S. B. Trier, R. M. Rasmussen, G. J. Holland, and M. P. Clark, 2017: Increased rainfall volume from future convective storms in the US. *Nat. Climate Change*, **7**, 880–884, https://doi.org/10.1038/s41558-017-0007-7.

——, R. M. Rasmussen, D. Wang, and S. E. Giangrande, 2021: Sensitivity of organized convective storms to model grid spacing in current and future climates. *Philos. Trans. Roy. Soc.*, **A379**, 20190546, https://doi.org/10.1098/rsta.2019.0546.

Rasmussen, K. L., A. F. Prein, R. M. Rasmussen, K. Ikeda, and C. Liu, 2020: Changes in the convective population and thermodynamic environments in convection-permitting regional climate simulations over the United States. *Climate Dyn.*, **55**, 383–408, https://doi.org/10.1007/s00382-017-4000-7.

Raupach, T. H., and Coauthors, 2021: The effects of climate change on hailstorms. *Nat. Rev. Earth Environ.*, **2**, 213–226, https://doi.org/10.1038/s43017-020-00133-9.

Robinson, E. D., R. J. Trapp, and M. E. Baldwin, 2013: The geospatial and temporal distributions of severe thunderstorms from high-resolution dynamical downscaling. *J. Appl. Meteor. Climatol.*, **52**, 2147–2161, https://doi.org/10.1175/JAMC-D-12-0131.1.

Schumacher, R. S., and K. L. Rasmussen, 2020: The formation, character and changing nature of mesoscale convective systems. *Nat. Rev. Earth Environ.*, **1**, 300–314, https://doi.org/10.1038/s43017-020-0057-7.

Seeley, J. T., and D. M. Romps, 2015: The effect of global warming on severe thunderstorms in the United States. *J. Climate*, **28**, 2443–2458, https://doi.org/10.1175/JCLI-D-14-00382.1.

Shepherd, T. J., F. L. Letson, R. J. Barthelmie, and S. C. Pryor, 2021: How well are hazards associated with derechos reproduced in regional climate simulations? *Nat. Hazards Earth Syst. Sci.*, **2021**, 1–42, https://doi.org/10.5194/nhess-2021-373.

Sherburn, K. D., and M. D. Parker, 2014: Climatology and ingredients of significant severe convection in high-shear, low-CAPE environments. *Wea. Forecasting*, **29**, 854–877, https://doi.org/10.1175/WAF-D-13-00041.1.

——, ——, J. R. King, and G. M. Lackmann, 2016: Composite environments of severe and nonsevere high-shear, low-CAPE convective events. *Wea. Forecasting*, **31**, 1899–1927, https://doi.org/10.1175/WAF-D-16-0086.1.

Sheridan, P., 2018: Current gust forecasting techniques, developments and challenges. *Adv. Sci. Res.*, **15**, 159–172, https://doi.org/10.5194/asr-15-159-2018.

Skamarock, W. C., and Coauthors, 2019: A description of the Advanced Research WRF Model version 4.1. NCAR Tech. Note NCAR/TN-556+STR, 162 pp., https://doi.org/10.5065/1dfh-6p97.

Smith, A., N. Lott, and R. Vose, 2011: The integrated surface database: Recent developments and partnerships. *Bull. Amer. Meteor. Soc.*, **92**, 704–708, https://doi.org/10.1175/2011BAMS3015.1.

Smith, A. B., and R. W. Katz, 2013: US billion-dollar weather and climate disasters: Data sources, trends, accuracy and biases. *Nat. Hazards*, **67**, 387–410, https://doi.org/10.1007/s11069-013-0566-5.

Smith, B. T., R. L. Thompson, J. S. Grams, C. Broyles, and H. E. Brooks, 2012: Convective modes for significant severe thunderstorms in the contiguous United States. Part I: Storm classification and climatology. *Wea. Forecasting*, **27**, 1114–1135, https://doi.org/10.1175/WAF-D-11-00115.1.

——, T. E. Castellanos, A. C. Winters, C. M. Mead, A. R. Dean, and R. L. Thompson, 2013: Measured severe convective wind climatology and associated convective modes of thunderstorms in the contiguous United States, 2003–09. *Wea. Forecasting*, **28**, 229–236, https://doi.org/10.1175/WAF-D-12-00096.1.

Squitieri, B. J., A. R. Wade, and I. L. Jirak, 2023a: A historical overview on the science of derechos. Part 1: Identification, climatology, and societal impacts. *Bull. Amer. Meteor. Soc.*, **104**, E1709–E1733, https://doi.org/10.1175/BAMS-D-22-0217.1.

——, ——, and ——, 2023b: A historical overview on the science of derechos. Part II: Parent storm structure, environmental conditions, and history of numerical forecasts. *Bull. Amer. Meteor. Soc.*, **104**, E1734–E1763, https://doi.org/10.1175/BAMS-D-22-0278.1.

Stensrud, D. J., M. C. Coniglio, R. P. Davies-Jones, and J. S. Evans, 2005: Comments on "'A theory for strong long-lived squall lines' revisited". *J. Atmos. Sci.*, **62**, 2989–2996, https://doi.org/10.1175/JAS3514.1.

Suomi, I., S.-E. Gryning, R. Floors, T. Vihma, and C. Fortelius, 2015: On the vertical structure of wind gusts. *Quart. J. Roy. Meteor. Soc.*, **141**, 1658–1670, https://doi.org/10.1002/qj.2468.

Surowiecki, A., and M. Taszarek, 2020: A 10-year radar-based climatology of mesoscale convective system archetypes and derechos in Poland. *Mon. Wea. Rev.*, **148**, 3471–3488, https://doi.org/10.1175/MWR-D-19-0412.1.

Theodoridis, S., and K. Koutroumbas, 2003: *Pattern Recognition*. Academic Press, 689 pp.

Thompson, G., P. R. Field, R. M. Rasmussen, and W. D. Hall, 2008: Explicit forecasts of winter precipitation using an improved bulk microphysics scheme. Part II: Implementation of a new snow parameterization. *Mon. Wea. Rev.*, **136**, 5095–5115, https://doi.org/10.1175/2008MWR2387.1.

Tippett, M. K., J. T. Allen, V. A. Gensini, and H. E. Brooks, 2015: Climate and hazardous convective weather. *Curr. Climate Change Rep.*, **1**, 60–73, https://doi.org/10.1007/s40641-015-0006-6.

Trapp, R. J., and K. A. Hoogewind, 2016: The realization of extreme tornadic storm events under future anthropogenic climate change. *J. Climate*, **29**, 5251–5265, https://doi.org/10.1175/JCLI-D-15-0623.1.

——, D. M. Wheatley, N. T. Atkins, R. W. Przybylinski, and R. Wolf, 2006: Buyer beware: Some words of caution on the use of severe wind reports in postevent assessment and research. *Wea. Forecasting*, **21**, 408–415, https://doi.org/10.1175/WAF925.1.

——, N. S. Diffenbaugh, H. E. Brooks, M. E. Baldwin, E. D. Robinson, and J. S. Pal, 2007: Changes in severe thunderstorm environment frequency during the 21st century caused by anthropogenically enhanced global radiative forcing. *Proc. Natl. Acad. Sci. USA*, **104**, 19 719–19 723, https://doi.org/10.1073/pnas.0705494104.

——, ——, and A. Gluhovsky, 2009: Transient response of severe thunderstorm forcing to elevated greenhouse gas concentrations. *Geophys. Res. Lett.*, **36**, L01703, https://doi.org/10.1029/2008GL036203.

——, E. D. Robinson, M. E. Baldwin, N. S. Diffenbaugh, and B. R. J. Schwedler, 2011: Regional climate of hazardous convective weather through high-resolution dynamical downscaling. *Climate Dyn.*, **37**, 677–688, https://doi.org/10.1007/s00382-010-0826-y.

——, K. A. Hoogewind, and S. Lasher-Trapp, 2019: Future changes in hail occurrence in the United States determined through convection-permitting dynamical downscaling. *J. Climate*, **32**, 5493–5509, https://doi.org/10.1175/JCLI-D-18-0740.1.

USGCRP, 2023: *Fifth National Climate Assessment*. U.S. Global Change Research Program, 1834 pp., https://doi.org/10.7930/NCA5.2023.

Weisman, M. L., and R. Rotunno, 2004: "A theory for strong long-lived squall lines" revisited. *J. Atmos. Sci.*, **61**, 361–382, https://doi.org/10.1175/1520-0469(2004)061<0361:ATFSLS>2.0.CO;2.

Weiss, S. J., J. A. Hart, and P. R. Janish, 2002: An examination of severe thunderstorm wind report climatology: 1970–1999. Preprints, *21st Conf. on Severe Local Storms*, San Antonio, TX, Amer. Meteor. Soc., 11B.2, https://ams.confex.com/ams/pdfpapers/47494.pdf.

Whittaker, L. M., and L. H. Horn, 1984: Northern Hemisphere extratropical cyclone activity for four mid-season months. *J. Climatol.*, **4**, 297–310, https://doi.org/10.1002/joc.3370040307.

Zhang, H., Z. Pu, and X. Zhang, 2013: Examination of errors in near-surface temperature and wind from WRF numerical simulations in regions of complex terrain. *Wea. Forecasting*, **28**, 893–914, https://doi.org/10.1175/WAF-D-12-00109.1.